RSC Advances

REVIEW

View Article Online
View Journal | View Issue

Cite this: *RSC Adv.*, 2024, **14**, 24604

Classification, synthesis, characterization, and applications of metal nanoparticle-containing hybrid microgels: a comprehensive review

Muhammad Arif, *[a] Hamid Raza[a] and Toheed Akhter*[b]

Received 5th June 2024
Accepted 4th July 2024

DOI: 10.1039/d4ra04128c

rsc.li/rsc-advances

In the last ten years, there has been significant interest in the integration of metal nanoparticles (MNPs) in smart microgels (SMGs). These combined structures of metal nanoparticles and smart microgels possess unique behaviors that make them suitable for a wide range of applications in catalysis, environmental and biological fields. The intrinsic responsiveness of microgels within these hybrid systems shows significant potential for application across multiple fields. Extensive literature provides diverse insights into the morphologies and compositions of metal nanoparticles in microgels. The design of these hybrid microgels plays a crucial role in determining their applicability, leading to tailored solutions for specific purposes under specific conditions. This review aims to summarize the latest advancements in the classification, synthesis, responsiveness, characterizations, and applications of hybrid microgel systems. Additionally, it explores the recent advancements in the applications of metal nanoparticle-decorated microgels in catalysis, adsorption, sensing, biomedical and environmental fields.

1. Introduction

Crosslinked networks that have the capacity to absorb a suitable solvent and thereby transform them from a deswelling state to a swelling state are called gels.[1] If the swelling/deswelling behavior occurs in an aqueous medium, the gel is called

[a]*Department of Chemistry, School of Science, University of Management and Technology, Lahore 54770, Pakistan. E-mail: Muhammadarif2861@yahoo.com; Muhammadarif@umt.edu.pk*

[b]*Department of Chemical and Biological Engineering, Gachon University, Seongnam 13120, Republic of Korea. E-mail: toheed@gachon.ac.kr*

Muhammad Arif

Dr Muhammad Arif has been Professor (Assistant) of Chemistry in the Department of Chemistry, University of Management and Technology, Lahore, since 2022. He was previously a lecturer in Chemistry in the Department of Chemistry, School of Science, University of Management and Technology, Lahore, from 2017 to 2022. He received his PhD in Chemistry from the University of The Punjab, Lahore, Pakistan. He obtained his M.Phil in Chemistry and MSc in Organic Chemistry from Quaid-i-Azam University Islamabad, Islamabad, and the Institute of Chemistry, University of the Punjab, Lahore, Pakistan, respectively. His research area includes the synthesis, characterization and applications of metal nanoparticle-fabricated microgels and ligands.

Hamid Raza

Dr Hamid Raza is a researcher in the field of MOFs, currently serving as Associate Professor in the Department of Chemistry and Dean at the Center for Teaching and Learning (CTL) at the University of Management and Technology (UMT), Lahore. He holds a PhD from UET, an M.Phil. from FCCU, an MSc. in Chemistry from Punjab University, an M.S. Ed from IER (PU), and a BSc from GCU, Lahore. His research spans materials science, environmental sustainability, and biotechnology, focusing on water purification, carbon capture, and photocatalytic activity. With 280 citations, an h-index of 9, and an i10-index of 9, Dr Raza's work is widely recognized. Published in diverse journals with a cumulative impact factor of 71.02, his contributions significantly advance the understanding and addressing of critical issues in these fields.

a hydrogel.[2,3] Further, gels falling in the three-dimensional micro-range diameter are termed microgels[4,5] and have emerged as a focal point of research interest over the past decade owing to their versatile applications.[6–8] Furthermore, microgels that show deswelling and swelling behaviors under external stimuli are termed smart microgels (SMGs).[9–11] This stimuli-responsive behavior of microgels creates a potential in their structure, which is essential for various applications in catalysis,[12–14] adsorption,[15,16] biomedicine,[17–19] and nanotechnology.[20–22] These applications are greatly affected by the rapid response of smart microgels to external stimuli, such as the ionic strength,[23,24] temperature,[25–27] and pH[28,29] of the medium, through their swelling/deswelling behavior. Moreover, extensive research has been conducted on microgels as micro-reactors, focusing on their ability to fabricate and stabilize inorganic particles (IPs).[30–32] These inorganic particles such as metal oxides, including SiO_2 and Fe_2O_3; metal sulfides; and metal nanoparticle-containing microgels are called hybrid microgels (HMGs). Among these hybrid microgels, metal nanoparticle (MNP)-containing microgels are an important type due to the easy identification, high catalytic performance, very small size, and large surface area of the metal nanoparticles in the microgels.

MNPs have various applications in different fields,[33–36] but their poor stability limits their long-term usage. To address this limitation, different types of stabilizers have been reported in the literature, such as microgels,[37] dendrimers,[38] block polymers,[39] and surfactants.[40] Among these, microgels have demonstrated significant potential in maintaining the stability of MNPs over prolonged periods[41–43] in addition to enhancing their performance.[44,45] Consequently, they are suitable candidates for the production and stabilization of MNPs. In this review article, hybrid microgels represent microgels incorporated with MNPs. Hybrid microgels are very important with respect to their superior catalytic activity.[46] These systems have the properties of both the metal nanoparticles and crosslinked polymer microgels. As they possess the properties of both components, hybrid microgels can be used for various applications, including drug delivery,[47] anticancer,[48] antibacterial,[49] adsorption,[50] sensing,[33] and catalysis.[51]

Toheed Akhter

Dr Toheed Akhter, PhD, is Assistant Professor at Gachon University, South Korea, specializing in polymer and porous materials. He completed his PhD jointly at KIAST, South Korea, and Quaid-i-Azam University, Pakistan. Dr Akhter has held postdoctoral positions at KAIST and UNIST, South Korea, and previously served as Assistant and Associate Professor at UMT, Pakistan. His research focuses on synthesizing and characterizing innovative materials for diverse applications.

A lot of research work has been done on these hybrid systems. As part of this, some researchers have published some reviews on single-metal-nanoparticles-loaded microgels,[52–55] but to the best of our knowledge, no review article has yet provided all the information on all types of metal nanoparticles-loaded microgel systems that have been developed in the last decade. Therefore, this review article is very important to new researchers because it provides all the information related to metal nanoparticles-decorated microgel systems.

2. Classifications

Metal nanoparticles embedded within microgels are categorized into different classes based on (i) the nature of the metal nanoparticles present in the microgels, and (ii) the morphologies of the hybrid microgels. Further information related to these classifications is given below.

2.1. Types of metal nanoparticles in smart microgels

On the basis of the metal nanoparticles incorporated in the system, the hybrid microgels can be classified into two classes as: (i) noble metal nanoparticles integrated into microgels (ii) non-noble metal nanoparticles integrated into microgels. These two classes of metal nanoparticles have a significant influence on the applications of hybrid systems. We discuss these classes below.

2.1.1. Noble metal nanoparticles integrated into microgels. Based on the Scopus database, it appears that there has been more work on noble metal nanoparticles integrated into microgels than non-noble metal nanoparticles integrated into microgels, likely due to the higher performance of noble metal nanoparticles than non-noble metal nanoparticles. Regarding noble metal nanoparticles, Ag and Au nanoparticles-containing hybrid systems have been frequently reported in the literature, while there are less reports on other noble metal nanoparticles-containing hybrid systems. The reason for the frequent reports on these two noble metal nanoparticles is their interesting surface plasmon resonance property. Due to this property, the identification of these two metal nanoparticles can easily be achieved and they can be monitored using a spectrophotometer. Their surface plasmon resonance wavelengths (λ_{SPR}) also provide information related to the shape and size of the particles; where the λ_{SPR} value for Ag nanoparticles occurs at approximately at 430 nm (ref. 56) and for Au nanoparticles it is approximately at 520 nm.[57] If a hybrid microgel shows a single peak in its UV-Vis spectrum, then spherical nanoparticles are present; while if two peaks appear in the spectrum, then the shape of the nanoparticles is rod-like. For example, Arif *et al.*[43] synthesized Au nanoparticles-based core–shell hybrid microgels. They obtained a single peak for λ_{SPR} at 521 nm, which indicated the presence of spherical-shaped Au nanoparticles. For clarification of this point, they also performed TEM analysis, which confirmed that the Au nanoparticles in the core–shell systems were spherical in shape. Similarly, Naseem *et al.*[58] also synthesized Ag nanoparticles-based core–shell hybrid microgels and investigated their optical properties. They

observed a single peak for λ_{SPR} at 440 nm, which together with the TEM results, indicated that the Ag nanoparticles were spherical in shape.

Noble metal nanoparticles-containing hybrid systems have frequently been used as catalysts due to their high catalytic activity,[59–61] which is due to their small size, high surface area, and easily oxidizing ability. Their catalytic activity can also be tuned under various stimuli conditions.[56] These conditions affect the swelling and deswelling behavior of the hybrid microgels. In the swelling state, reactant molecules can easily reach the surfaces of the nanoparticles, which are the actual catalytic materials in the hybrid microgels. Therefore, reduction or degradation or transformation reactions occur rapidly. Conversely, the reactant diffusion rate decreases in the deswelling state, and therefore less reactant molecules reach the surface of nanoparticles, which is why the reaction rate decreases. The factors that can tune this catalytic performance are the temperature,[62] pH,[63] and ionic strength.[64]

These hybrid systems are also used as adsorbent for pollutants.[65–67] The adsorption capacity of these hybrid systems depends on the nature of the polymer components. Specifically, the nature of the monomers and comonomers determines their selectivity for the adsorption of pollutants. This selectivity can be tuned by the pH of the medium for acidic and basic hybrid microgels. In a low pH medium, acidic hybrid microgels are present in protonated forms and are deprotonated at high pH values. In the deprotonated form, negative charge is present in the structure of the hybrid microgels. Therefore, hybrid microgels can attract positively charged pollutants but remove anionic pollutants *via* electron static interactions and repulsions, respectively. Similarly, basic hybrid microgels can also be produced selectivity for the adsorption of pollutants by varying the pH value of the medium.

Hybrid microgels are also used for drug delivery.[47] This behavior also depends on the swelling and deswelling behavior of the crosslinked networks of microgels.[21] Typically, the drug is loaded into the hybrid microgels in their swelling state and released by transforming them into their deswelling state. During this conversion, the loaded drug comes out along with water molecules. This conversion is done on the basis of the stimuli conditions. Au-based hybrid microgels are the best in this regard due to the ability of Au nanoparticles to convert light into heat. This property facilitates the release of the loaded drug from hybrid systems.[68] For Au-based hybrid microgels, an anticancer drug could be loaded into the system and injected into the body. When the drug-loaded hybrid microgels reach the target place, then laser light is applied to this drug-loaded hybrid system. The Au nanoparticles absorb the laser light and convert it into heat. Due to this conversion, the temperature of the medium rises and the hybrid microgels transform from the swelling state to the deswelling state and release the loaded drug. In this way, no surgery is required for the patent and the maximum release of the loaded drug occurs at the target place only. Au-based hybrid microgels are mostly the ones used for anticancer treatment.

Typically, such hybrid systems also have efficient antibacterial activity.[69,70] Therefore, these hybrid systems are used for different biological fields. This property generally depends on the nature of the metal nanoparticles. These nanoparticles can kill bacteria to control certain diseases. The efficiency of such hybrid systems can be controlled by controlling the release or approach of bacteria to the surface of the noble metal nanoparticles.

These hybrid microgels can also be used as sensors for the identification of different pollutants in water.[71–73] During the sensing process, the oxidation state of the metal nanoparticles varies, or complexation takes place with the crosslinked network of the hybrid microgels. For example, Au-based hybrid microgels have been used for sensing albumin, mercuric ions, glucose levels, and some others. Similarly, other noble metal nanoparticles-based hybrid microgels can also be used for sensing different types of pollutants.

Noble metal nanoparticles-based hybrid systems are the most effective systems compared to the others due to their high performance and high stability. However, one limitation may be the cost effect of noble metal nanoparticles-based hybrid microgels. This issue can be resolved by using bimetallic nanoparticles-based hybrid systems. In these systems, cheaper metal nanoparticles are mixed with noble metal nanoparticles to reduce the cost. Another limitation is that the identification of noble metal nanoparticles (except Ag and Au) in microgels cannot be done with simple characterization techniques, such as FTIR, UV-Visible spectrophotometry, and their confirmation instead requires more costly instruments and techniques, such as TEM and HR-TEM. This issue can also be resolved by using bimetallic systems, in which Au or Ag nanoparticles are just one component. These systems have been reported for the transformation of some reactants, while others can also be converted into other suitable molecules by these hybrid systems. There are very limited adsorption studies on these systems reported in the literature, and more research work will be needed on these systems in the near future.

2.1.2. Non-noble metal nanoparticles integrated into microgels. Besides noble metals, there are other transition metal nanoparticles-based hybrid microgels, which are called non-noble metal nanoparticles. These types of hybrids contain cheaper metal nanoparticles, where the price of these metals is very low. However, the stability of these metal nanoparticles is also typically very low. There is less research work on non-noble metal nanoparticles-based hybrid microgels than noble metal nanoparticles due to their poor performance and low stability.[74,75] The most study has been done on Fe and Cu nanoparticles-based hybrid microgels compared to other non-noble metals.

These metal nanoparticles do not show λ_{SPR} values in UV-Visible spectrophotometry because they do not have surface plasmon resonance frequency. Therefore, the presence of these metal nanoparticles cannot be confirmed by simple instruments.

Also, while these systems show good catalytic performance, their efficiency is low compared to noble metal nanoparticles due to their high surface area, low oxidizing property, and large particles sizes.[43,50] Further, the catalytic performance of these hybrid microgels can also be tuned under different stimuli

conditions similar to noble metal nanoparticles-based hybrid microgels. However, their catalytic performance rapidly decreases with increasing the storage time of hybrid microgels after synthesis, but can be increased from days to weeks with the help of the crosslinked networks of microgels, though even then their stability is still less than that of noble metal nanoparticles-based hybrid microgels. Further, coagulation can occur in metal nanoparticles, which decreases the surface area of the metal nanoparticles of hybrid microgels.

These hybrid microgels can be used for the adsorption of pollutants, but their adsorption capacity is less than that of microgels.[76,77] Basically, the adsorption capacity depends on the empty space present in the crosslinked network of the microgels. This space decreases after the incorporation of metal nanoparticles, and therefore, the adsorption capacity decreases.

Non-noble metal nanoparticles do not have the ability to convert light into heat, as Au nanoparticles have. Therefore, they are less applicable for drug delivery, but their tuning behavior still makes these hybrid microgels suitable for certain drug delivery.[78] The coagulation of metal nanoparticles is the main drawback for this application due to it reducing the empty space. These hybrid microgels can also be used for antibacterial activity. This property of these hybrid microgels is helpful for treatment against different diseases.

Less research work has been done on these hybrid microgels with respect to drug delivery, antibacterial applications, and the adsorption of pollutants. Therefore, more research work is needed to gain more information on these, such as research work on the stability of these metal nanoparticles. This further work could help to overcome their current drawbacks. Also, as their performance can be controlled by controlling the size of the particles, if such conditions could be obtained, then these systems may be a superior option to noble metal nanoparticles-based hybrid systems due to their lower cost and higher surface area. Further, their performance can be enhanced by using bimetallic nanoparticles-based hybrid microgels, as reported in our previous review article.[79]

2.2. Morphology-based classifications of hybrid microgels

Various designs of hybrid microgels have been reported in the literature, and hybrid microgels can be classified into various classes based on their morphology, as given below.

2.2.1. Core–shell hybrid microgels. Much current research is focused on core–shell hybrid microgels. These can be further categorized into sub-classes based on the species and their positions within the structure of the hybrid microgels.

2.2.1.1. Metal nanoparticles encapsulated by polymer microgels. In such categories, metal nanoparticles (MNPs) are present at the center (core), surrounded by polymer microgels (shell), as shown in Fig. 1(a). These core–shell hybrid microgels (HMGs) typically exhibit low catalytic activity. The diffusion rate of the reactant molecules from the outer region to the surface of MNPs through the crosslinked polymeric network is notably slow due to the long distance between them. Therefore, the approach of reactant molecules takes more time.[75,80] Consequently, the catalytic efficiency of these HMGs is very low compared to other classes of HMGs. However, the stability of MNPs is greater in these systems, and the leaching of metal nanoparticles is not possible in these systems during their recovery by centrifugation after their catalytic application. Such systems can also be used for drug delivery due to the polymeric network. Polymeric

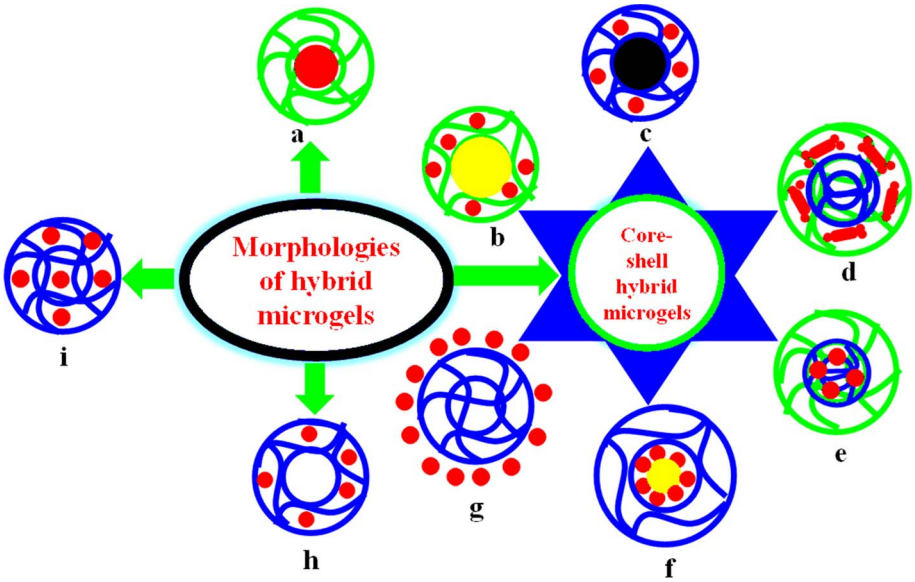

Fig. 1 Morphological classifications of hybrid microgels (metal nanoparticles are represented by red color; inorganic materials by black color; and organic polymers by green, blue and yellow colors). (a) Metal nanoparticle-encapsulated polymer microgels, (b) organic polymer-encapsulated MNPs decorated with crosslinked polymers, (c) inorganic-encapsulated MNPs decorated with polymer microgels, (d) organic polymer-encapsulated bimetallic NPs decorated with polymer microgels, (e) MNP-decorated organic polymer encapsulated in another organic polymer, (f) organic polymer-encapsulated MNP layer encapsulated in another organic polymer, (g) organic polymer-encapsulated metal nanoparticles, (h) MNPs in hollow microspheres and (i) homogenous hybrid microgels.

networks have polar functional groups in their structure, and these polar components interact with the water molecules as well as the drug. If the interaction between the drug and the HMG is strong, then more drug can be loaded in these systems. Conversely, these systems are highly advantageous for drug-delivery purposes due to their high drug-loading capacity. Similarly, these systems show adsorption properties for various pollutants due to interactions between the crosslinked network and certain pollutants. They can be further categorized into two classes based on the use of (i) monometallic nanoparticles[81] or (ii) bimetallic nanoparticles.[82] Bimetallic nanoparticles-based HMGs show greater performance than monometallic systems due to the synergistic effects the bimetallic components.

Only gold (Au)[44,83] and silver (Ag)[84] nanoparticles encapsulated in microgels have been reported for monometallic nanoparticles encapsulated within microgels. Additionally, Au,[80] Ag,[75] and Co/Ni[85] have also been reported as bimetallic nanoparticles within microgels, exhibiting identical morphologies. To date, both variants of these categories have been utilized solely for their catalytic activity, and their potential for applications in drug delivery and other biological aspects have not yet been reported in the literature. Moreover, they can be utilized as adsorbents for various pollutants found in water and the environment. These classes and potential application represent viable opportunities for further research on these types of hybrids.

2.2.1.2. Organic polymer-encapsulated MNPs decorated by crosslinked polymers. In these categories, an organic core is encased within another crosslinked polymer shell and the metal nanoparticles are located in the shell region of the core–shell microgels, as shown in Fig. 1(b). Organic polymer-encapsulated MNPs decorated by crosslinked polymer systems have greater significance than MNPs-encapsulated microgel systems due to their superior catalytic activity[86,87] and greater density of HMGs. Actually, the distance between the reactant molecules and the surface of metal nanoparticles is minimized in the former scenario compared to in the lateral HMGs. However, the lateral systems tend to exhibit a higher drug-loading capacity than the former systems due to the occupation of the space by the metal nanoparticles, resulting in a low empty space for drugs in the former HMG systems. The catalytic efficiency and drug-loading capacity of both types of systems can be enhanced by altering the environment of the medium. The crosslinked network of HMGs can transform from a deswelling state to a swelling state with the aid of stimuli. Additionally, the easy recyclability (due to greater density) of these systems is another advantage. These systems can be further classified into two categories based on the incorporation of (i) monometallic nanoparticles[88] or (ii) bimetallic nanoparticles[89] in the core–shell microgels, as shown in Fig. 1(e). Bimetallic systems yield superior results for catalysis and surface-enhanced Raman scattering due to synergistic effects of the bimetallic components.

Monometallic (Au,[43] Cu,[50] Pd,[86] Ni,[90] Ag,[91] and Pt[92]) nanoparticles-based core–shell hybrid microgels have been documented in the literature. Similarly, the incorporation of bimetallic nanoparticles (Pt,[89] Au,[93] Ag,[94] and Pd[95]) within core–shell microgel systems has also been documented in the literature. Only Cu-based monometallic nanoparticles-based hybrid microgels of this class have been reported to date, while bimetallic systems of non-noble metal nanoparticles-based HMGs have not been reported yet. This thus represents an available space for further research work. These systems are commonly employed as catalysts, but their potential as adsorbents for various pollutants or in biological applications has not yet been reported. Additionally, the influence of the core on the leaching of metal nanoparticles in these hybrid systems has not been studied yet, presenting another area for further research.

2.2.1.3. Inorganic-encapsulated MNPs decorated by polymer microgels. In these classes, the core is composed of inorganic materials, like Fe_2O_3, SiO_2, or Fe_3O_4, which is encapsulated with a metal nanoparticles-containing microgel shell, as shown in Fig. 1(c). These hybrid microgels in which a paramagnetic inorganic core is surrounded by metal nanoparticles within microgels have significant importance due to their enhanced recyclability compared to other systems. These HMGs can be efficiently recycled using magnetic fields[96] or centrifugation processes.[97] During this recycling (*e.g.*, recycling by a magnetic field), the issue of the leaching of metal nanoparticles from the crosslinked network can be solved by these hybrid microgels. Additionally, they can serve as catalysts for various catalytic reactions. However, the stimuli-responsive behavior of such systems slightly is diminished compared to that of pure microgel systems due to the presence of solid inorganic species; whereby these solid species decrease the effects of pH, temperature, and ionic strength on these hybrid microgels due to the formation of an interface between the solid inorganic core and the crosslinked organic polymer microgels.[9] Despite their significance, such systems have not been frequently documented in the literature. However, they can be used for drug delivery and the adsorption of pollutants, where their easy recyclable property makes these HMGs suitable for these applications. They can also be applicable for antibacterial applications. Further, these types of HMGs can be divided into a further two classes: (i) mono-inorganic material-encapsulated MNPs decorated by crosslinked polymers[30] and (ii) bi-inorganic material-encapsulated MNPs decorated by crosslinked polymers.[98] Bi-inorganic materials containing core–shell hybrid microgels are better than monometallic ones due to their high density, easy recyclable property, and the synergistic effect of the bi-inorganic components.

Mono-inorganic material-encapsulated MNPs-decorated crosslinked polymer systems have been reported with different noble metal nanoparticles-based hybrid systems, such as Au,[96] Ni,[30] Ag,[97] and Pd,[99] but not reported for non-metal nanoparticles-based hybrid microgels, while bi-inorganic material-encapsulated MNPs-decorated crosslinked polymer systems have been reported with monometallic Co[100] nanoparticles only. Controlling the size of the core is the main issue in these types of hybrids. This issue can be controlled by adding a stabilizer along with the formation of crosslinked polymers. Hybrid microgels of these types are mostly applied for catalytic reactions, while the other environmental and biological fields seem to have no research performed yet. Furthermore, these hybrid microgels have not been synthesized with bimetallic

nanoparticles, and so this may be a good option for further research. Further research efforts could thus be directed toward exploring and developing these types of hybrid microgels.

2.2.1.4. MNPs-decorated organic polymer encapsulated by another organic polymer. In systems of MNPs-decorated organic polymers encapsulated by another organic polymer, both the core and shell systems of the hybrid microgels consist of crosslinked organic polymers, and metal nanoparticles are present in the core region of these hybrid core–shell systems, as shown in Fig. 1(e). These types of HMGs are very effective for controlling the leaching of metal nanoparticles during the centrifugation recycling process. These hybrid microgels can be used for catalytic reactions, but their catalytic activity is lower than other classes. However, their catalytic efficiency can be tuned with the help of external stimuli conditions.[13,101] These conditions control the swelling and deswelling behavior of the shell region, which can permit the entrance of reactant molecules. These reactant molecules reach the metal nanoparticles through the shell region. Therefore, their swelling behavior is very important for the catalytic efficiency of these types of core–shell systems. The shell region can also be used for the adsorption of other pollutants. In this way, these types of HMGs are excellent candidates for both adsorption as well as catalysis. They can also be employed for drug delivery and the loading and release of a drug can be controlled by the stimuli-responsive shell region. Also, if the nanoparticles are based on Au nanoparticles, then it is an excellent drug carrier system, because Au nanoparticles can control the deswelling behavior of the shell region by converting applied light into heat. Also, during this conversion, the shell region or core region transforms from a swelling to deswelling state. If the drug is loaded in the core region, then the deswelling of the shell region controls the release of the drug, and if the drug is present in the shell region, then it comes out along with the water molecules during this transformation. The antibacterial activity of these hybrid microgels is lower than in previous classes due to their low diffusion rate and possible leaching of metal nanoparticles.

Systems of MNPs-decorated polymers encapsulated by another organic polymer have been documented with only Pd[13] and Au[102] nanoparticles, and bimetallic nanoparticle-based hybrid systems of this class have not been reported yet. Furthermore, these hybrid microgels along with non-metal nanoparticles have also not been reported in the literature yet. Hence, there is a need for further research in these categories, as they are excellent candidates with cores for controlling the drug loading/release, catalytic reactions, and adsorption of pollutants. Additionally, there is available research space for exploring the synthesis of these kinds of hybrid microgels with other noble and non-noble metals with monometallic and bimetallic systems.

2.2.1.5. Organic polymer-encapsulated MNPs layer encapsulated by another organic polymer. In systems with an organic polymer-encapsulated MNPs layer encapsulated by another organic polymer, a core–layer–shell system of hybrid microgels are formed in which both the core and shell regions contain organic polymers and metal nanoparticles are present in-between these core and shell regions in the form of a layer, as shown in Fig. 1(f). This class of hybrid microgels has greater catalytic efficiency than MNPs-encapsulated crosslinked polymer systems and MNPs-decorated organic polymers encapsulated by another crosslinked organic polymer systems, but less than other classes of hybrid microgels due to the approaches of the reactant molecules to the MNPs' surface. Their catalytic activity can also be tuned by the stimuli conditions. The leaking capacity of MNPs in these hybrid microgels is minimum during recycling, which is performed by a centrifugation process. The adsorption capacity of these hybrid systems is high due to the direct contact of pollutants with the crosslinked networks. The adsorption capacity of these hybrid microgels depends on the nature of the adsorbate and the nature of monomers and comonomers in the structure of hybrid microgels, because the strength of interactions between pollutants and the hybrid microgels depends on the nature of both the pollutants and hybrid microgels. They are also applied for drug delivery, similar to the adsorption of pollutants. The loaded drug can be released during the conversion from the swelling state of the hybrid microgels to the deswelling state. This drug release can be controlled by altering the interaction strength between the drug and hybrid microgels *via* the stimuli conditions.[103]

Very limited research work has been done on systems involving an organic polymer-encapsulated MNPs layer encapsulated by another organic polymer. Only Au nanoparticles-based hybrid microgels are detailed in the literature.[104] There is thus an opportunity for further research to explore the synthesis of these types of hybrid systems with both types of metal (noble and non-noble) nanoparticles. Thus investigation into the adsorption, drug loading/release, and catalytic activity of these hybrid systems offers new ground for research.

2.2.1.6. Organic polymer-encapsulated metal nanoparticles. In organic polymer-encapsulated metal nanoparticles, the crosslinked network of the organic polymer is surrounded by metal nanoparticles, as shown in Fig. 1(g). These types of hybrid microgels are synthesized through electrostatic interactions between the microgel and metal nanoparticles.[71,105] The degree of coverage of the microgel surface with the metal nanoparticles depends on various factors, such as the charge density of the microgels, the crosslinking density, the polarity of the structure, and the porosity of the microgels. Modulating the concentration of ionic radical initiators or content of crosslinkers or content of charged comonomers during the polymerization process can facilitate the design of microgels with a high adsorption capacity of metal nanoparticles at their surface. Organic polymer-encapsulated metal nanoparticles exhibit the highest efficiency in catalytic reactions than other hybrid microgels due to the easy access of the reactant molecules to the metal nanoparticle surface. However, their catalytic efficiency rapidly diminishes during the recycling process, due to the detachment of metal nanoparticles from the surface of the microgels. After recycling, the content of metal nanoparticles on the surface of microgels decreases. Therefore, their catalytic activity decreases sharply after recycling. Moreover, these types of hybrids are not ideally suited to drug delivery due to the decrease in drug loading caused by the coverage of metal nanoparticles. Nonetheless, a few studies on drug delivery using

such systems have been published.[106] Karg *et al.*[107] reported a coating of P(NIPAM) microgels with gold nanorods. The resulting core–shell hybrid systems were obtained through electrostatic interactions between the gold nanorods and the microgels. Surface modification of both the gold nanorods and the microgels was necessary to induce these interactions, which could be conveniently achieved by increasing the concentration of free radical initiators or incorporating charged comonomers. Similarly, the gold nanorods needed to carry an opposite charge to the surface functionalities of the microgels. This was accomplished through the introduction of a polyelectrolyte bilayer to enhance the colloidal stability and create a positive charge on their surface. Mixing positively charged gold nanoparticles with negatively charged microgels resulted in the formation of core–shell hybrid microgels. Wong *et al.*[108] reported the synthesis of P(NIPAM) microgels modified with magnetic nanoparticles. These were obtained by surface modification of the microgels to enable the adsorption of magnetic nanoparticles *via* electrostatic interaction. In a study by Karg *et al.*,[109] it was demonstrated that copolymer microgels with charged surfaces could be efficiently coated with gold nanorods, leading to significant surface coverage. These charged microgels consisted of the poly(*N*-isopropyl acrylamide-allyl acetic acid) (P(NIPAM-AAAc)) system. A negative charge was created on the surface of these microgels at specific pH levels (in basic medium) due to the conversion of COOH groups into COO^- ions. This creation of charge established a strong electrostatic interaction between the surface-modified gold nanorods and anionic microgel surface. These hybrid microgels exhibited remarkable optical properties that were also responsive to external stimuli. The antibacterial activity of these hybrid microgels was also high due to the direct contact of bacteria with the metal nanoparticles.

Organic polymer-encapsulated monometallic (Pd,[71] Cu,[110] Au,[111] and Ag[105]) nanoparticles and bimetallic (Au,[112] and Pd[95]) systems have been documented in the literature. However, few articles are available on systems involving organic polymers encapsulated with bimetallic nanoparticles. The catalytic efficiency of organic polymer-encapsulated bimetallic nanoparticles is the highest among all other systems of hybrid microgels. After these systems, organic polymer-encapsulated monometallic nanoparticles are ranked in second place with respect to their catalytic performance. The catalytic activity and recycling properties of such systems thus warrant further investigation in the near future. The leakage and coagulation of metal nanoparticles is the main issue of these hybrid microgels. More study is needed on controlling the size of the metal nanoparticles as well as their application in adsorption and drug delivery.

2.2.2. MNPs in hollow microspheres. In systems comprising MNPs in hollow microspheres, the hollow microsphere is made with an organic crosslinked polymer and metal nanoparticles are present in these hollow microgels, as shown in Fig. 1(h). The hollow microsphere is formed by removing the core from core–shell polymer microgel systems. MNPs are then introduced into these hollow microspheres to form hollow microsphere hybrid systems.[113] The catalytic activity of these hybrid systems is greater than that of the previously discussed hybrid microgels. In these hybrid systems, pollutants can easily diffuse into the hybrid systems from both the interior and exterior sides. Therefore, there is a rapid diffusion rate. Consequently, the pollutants can rapidly reach the surface of the MNPs. The leaching of metal nanoparticles is the main issue with these types of hybrids. This issue can be resolved by using some paramagnetic nanoparticles along with MNPs in the hybrid systems. After the introduction of these (paramagnetic) nanoparticles, the MNPs in hollow microsphere can easily be recycled by using a magnetic field. These types of hybrids have high efficiency for the adsorption of pollutants. Therefore, MNPs in hollow microspheres are excellent for the adsorption of pollutants. Moreover, the hollow sphere hybrid microgels exhibit superior swelling/deswelling capacities compared to other core–shell hybrid microgels, making them effective for the loading and release of drugs from both the outer surface and the inner sides. Li *et al.*[114] described the synthesis of temperature-dependent hollow microspheres. They synthesized core–shell microgels with a poly(methylmethacrylic acid) (P(MMAAc)) core and a varying thickness shell based on P(NIPAM) at first. The P(MMAAc)-based core could be selectively removed from this core–shell system by a simple continuous stirring due to the high solubility of the core in the medium. He *et al.*[113] prepared hollow hybrid gold-based nanospheres by synthesizing a silica core and then introducing a shell composed of poly(2-(1-methylimidazolium 3-ethyl)-ethylmethacrylate chloride) (P(MIEEMACh)) first, followed by the production of gold nanoparticles by an *in situ* reduction. After that, the silica core was removed from the hybrid core–shell system by treatment with hydrofluoric acid. The resulting hollow hybrid temperature-dependent microspheres exhibited efficient catalytic efficiency toward the reductive reaction of 4NiP.

Hollow hybrid microspheres have been documented only with Au-[113] or Ag[114]-based hybrid microgels, and no work on non-noble metal nanoparticles in hollow microspheres has been reported in the literature. Therefore, further research could explore the utilization of other metal (both noble and non-noble) nanoparticles in these systems and their applications, such as in catalysis, drug delivery, and for the adsorption of various pollutants from water. Additionally, investigating the potential leaching of metal nanoparticles in such hybrid microgels is an area for future study. A comparison study of these hollow hybrid microgels would also be warranted comparing among themselves and with other core–shell hybrid systems.

2.2.3. Homogenous hybrid microgels. In homogenous hybrid microgels, metal nanoparticles are uniformly located within the meshes of the crosslinked polymer network of the microgels, as shown in Fig. 1(i). Homogenous hybrid microgels have been extensively documented in the literature.[61,115–121] These hybrid systems can serve as catalysts for various catalytic reactions. The synthetic approach of these hybrid microgels is easy compared to other hybrid microgels, like hollow microspheres, microgel-encapsulated metal nanoparticles, and all types of core–shell hybrid microgels. Consequently, numerous

studies have been reported on these classes of hybrid microgels. These hybrid microgels systems may also be applicable in drug delivery,[47,120,122] water pollutant adsorption,[123] sensing,[33] and antibacterial applications.[70,124,125] For instance, Zhang *et al.*[126] synthesized Ag NPs decorated by poly(*N*-isopropylacrylamide-maleate carboxymethylchitosan) (P(NIPAM-MCMCS)) microgels, and reported achieving a uniform dispersion of Ag NPs in the microgels. They used these hybrid systems for the catalytic reduction of nitroarenes. Liu *et al.*[127] synthesized a crosslinked structure of P(NIPAM) microgels by interpenetrating linear poly(acrylic acid) (P(AAc)) within them. The Ag nanoparticles were uniformly introduced into the crosslinked microgel network *via* an *in situ* reduction method. Additionally, Zhou *et al.*[128] reported the synthesis of Au-based hybrid microgel systems. They synthesized different samples with varying sizes of gold nanoparticles within the microgels by employing different concentrations of gold salts. These hybrid systems were then applied for the catalytic reduction of nitroarenes in aqueous media, with the reduction process observed to follow a pseudo-first-order kinetics.

Monometallic hybrid systems based on Au,[57] Co,[129] Pt,[130] Ni,[131] Ag,[59] Cu,[132] Rh,[133] Pd,[121] Fe,[134] and Ru[135] have been documented in the literature. Additionally, bimetallic systems incorporating Ag,[74] Fe,[136] Au,[137] Ni,[138] Pd,[13] Cu,[139] Pt,[140] and Co[141] nanoparticles have also been reported. These systems find extensive applications in catalysis, drug delivery, cancer treatment, adsorption, and antibacterial applications. Typically, the monomers and comonomers used in these hybrid systems are non-biodegradable. Hence, researchers can now focus on the further exploration of these systems by incorporating biodegradable monomers. Addressing the leaching of metal nanoparticles from these hybrid microgels is also an important area of research.

3. Synthesis

Several methods have been documented in the literature for the preparation of metal nanoparticles in microgels.[32,96,142–144] Specific synthetic methods may be applied based on the desired particular architecture, design, and morphology of the hybrid microgels. These synthetic approaches are outlined in Fig. 2(A)–(C).

3.1. Synthesis of metal nanoparticles in a microgel dispersion

A method commonly employed to synthesize metal nanoparticles in microgels is *via* the insertion of metal ions into the crosslinked network of microgels, followed by an *in situ* reduction these ions into their atomic forms, as shown in Fig. 2(A).[56,124,145–151] These atoms then start to coagulate up to the nano-range. The coagulation of metal atoms is controlled by the crosslinked network of the microgels. Control of the size distribution and dimensions of the metal nanoparticles can be achieved by adjusting the uniformity and pore size of the polymer network, whereby the size of the particles is controlled by the crosslinking density. If the crosslinking density of microgels is high, then small-sized metal nanoparticles are formed due to the low available space. While if the crosslinking density is low, then large sized particles are formed due to large available spaces in the structure of the microgels. In this approach, the structure of the microgels acts as a micro-reactor for nanoparticle synthesis. Whereby, the synthesized hybrid microgels can obtain a uniform distribution of metal nanoparticles throughout the structure. The content of monomers and comonomers are also controlled the size of MNPs. In this way, the composition of the microgels controls the incorporation of the metal content within their pores.

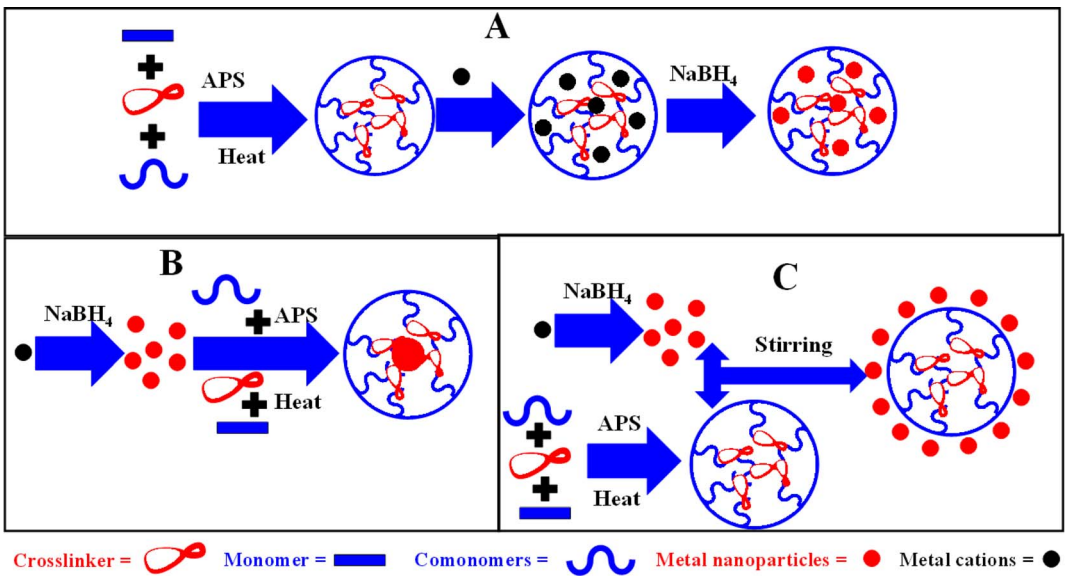

Fig. 2 Synthesis of hybrid microgels. (A) Synthesis of metal nanoparticles in a microgel dispersion, (B) synthesis of microgels in a solution of metal nanoparticles, and (C) hybrid microgel formation by simultaneously mixing microgels and metal nanoparticles.

Shah *et al.*[152] applied this methodology to produce Au nanoparticles within poly(*N*-isopropyl acrylamide-acrylic acid) P(NIPAM-AAc) microgels. The size and size distribution of the Au NPs were influenced by the ratio of AAc to NIPAM in the P(NIPAM-AAc) microgel composition. Additionally, they observed that the size of the Au nanoparticles could be manipulated by varying the stimuli conditions during synthesis. Furthermore, another study[98] reported on the synthesis of silver nanoparticles within poly(*N*-isopropylacrylamide-arylamide-methacrylic acid) P(NIPAM-AAm-MAAc) microgels. The synthesis involved two steps. In the first step, P(NIPAM-AAm-MAAc) microgels were synthesized by a free radical precipitation polymerization method. In this step, NIPAM (monomer), AAm (comonmer), MAAc (comonmer), *N*,*N*-methylenebis(acrylamide) (NMBA) (crosslinker), and sodium dodecyl sulfate (SDS) (stabilizer) were mixed and heated at 70 °C under nitrogen with vigorous stirring. After 30 min, ammonium persulfate (APS) (free radical initiator) solution was added and the reaction was continued for another 5 h under similar conditions. Silver salt solution was poured into the dispersion medium of P(NIPAM-AAm-MAAc). In the second step, these incorporated silver ions were subsequently transformed into silver nanoparticles *via* an *in situ* reduction method utilizing $NaBH_4$ as the reductant.

This method is simple and easy. It can be used for the synthesis of uniformly distributed MNPs in microgels. The size and distribution of the MNPs can be perfectly controlled by this method. Both monometallic (such as Au,[43] Ni,[153] Pt,[130] Co,[123] Ag,[119] Cu,[154] Pd,[155] Rh,[133] Fe,[156] Ru[135]) and bimetallic (including Pd,[139] Ni,[76] Pt,[89] Co,[157] Ag,[94] Cu,[158] Au[82]) hybrid microgels have been synthesized using similar approaches, as documented in the literature. The drawback of this approach is that core–shell hybrid microgels are not prepared.

3.2. Synthesis of microgels in a solution of metal nanoparticles

In this synthetic approach, a core–shell hybrid microgel system is formed, in which the core consists of metal nanoparticles and the shell of crosslinked organic polymers. This synthesis also proceeds *via* two steps. In the first step, metal nanoparticles are synthesized and stabilized using a stabilizer. In the second step, these synthesized metal nanoparticles are then used as seeds for the synthesis of the microgels, as shown in Fig. 2(B).[159–162] The surface of the metal nanoparticles can also be modified to produce polarity on the surface of the metal nanoparticles. This modified surface facilitates size control of the MNPs and the formation of microgels around these nanoparticles. The polymerization process occurs within a dispersion of metal nanoparticles, utilizing appropriate monomers, surfactants, initiators, comonomers, and crosslinkers under specific conditions. Li *et al.*[82] developed core–shell hybrid microgels with a bimetallic core and a shell based on *N*-isopropylacrylamide (NIPAM) using a slightly modified seed emulsion polymerization method. They applied silver nanoparticles stabilized with sodium citrate as seeds. The surface of the synthesized Ag nanoparticles was modified with NIPAM. Subsequently, Ag@poly(*N*-isopropylacrylamide-3-methacryloxypropyltrimethoxysilane) (Ag@P(NIPAM-MAPTMSi)) hybrid microgels were obtained by adding an aqueous solution of ammonium persulfate and 3-methacryloxypropyltrimethoxysilane. Furthermore, Ag-Au@P(NIPr-MAPTMSi) hybrid microgels were synthesized through a galvanic reaction (GRe) by utilizing the Ag-based hybrid system as a sacrificial template in an aqueous medium in the presence of aqueous ammonia. The by-product (AgCl) was removed from the reaction mixture using ammonia. Similarly, Bandyopadhyay *et al.*[144] employed a comparable approach to fabricate Au@P(NIPAM-AAc) hybrid microgels with a core–shell morphology, in which the core was composed of Au and the shell was made of P(NIPAM-AAc). They used polyethylene glycol P(EGl) to modify different morphologies of Au nanoparticles, which served as core particles for the copolymerization of NIPAM and acrylic acid (AAc), resulting in the formation of hybrid microgels.

This system is applicable for the synthesis of core–shell hybrid microgels only but not for homogenous hybrid microgels. More control of the performance and time are required in this method. This synthetic approach also has a drawback related to the size control of the metal nanoparticles, which is critical as the size of MNPs is the most important parameter for many their applications. Therefore, this method is less commonly used than the previously discussed methods. Monometallic (such as Au,[144] Ag[100]) hybrid microgels and bimetallic (Ag, Co, Ni, and Au[27]) hybrid systems are synthesized using similar approaches. Other hybrid systems based on metal nanoparticles (both monometallic and bimetallic) can be synthesized using this method.

3.3. Hybrid microgel formation by simultaneously mixing microgels and metal nanoparticles

In the third method, both microgels and metal nanoparticles are synthesized separately and are later combined to generate hybrid microgels, as shown in Fig. 2(C). Before the formation of hybrid microgels, the surface of MNPs must be modified to create polarity. These hybrid microgels are then synthesized through electrostatic interactions. The hydrophilic components of the microgels interact electrostatically with the metal nanoparticles.[33,163–168] This interaction facilitates the fabrication of the microgels system with the metal nanoparticles. During this fabrication, MNPs come into or onto the crosslinked network of the microgels. If the size of metal nanoparticles is greater than the sieves of the microgels, then they attach on the surface of the microgels to form hybrid systems; whereas if the size of the MNPs is slammer than the sieve area, then they fall into the crosslinked network. Liu *et al.*[96] described the formation of gold nanoparticles-based core–shell hybrid microgels through simultaneously mixing their solutions. They synthesized core–shell microgels with a core of Fe_3O_4 and a shell of a crosslinked network of P(NIPAM-DMAEMA). First, gold nanoparticles were synthesized, stabilized, and functionalized with trisodium citrate. Next, the separately synthesized and functionalized gold nanoparticles were loaded into the shell

region of the core–shell system through the aid of the electrostatic attractions between the functionalized Au nanoparticles and the polar network of the microgels. Similarly, Gu *et al.*[165] achieved a hybrid system by mixing a dispersion of microgels with gold nanoparticles. Mutharani *et al.*[71] reported a similar method for synthesizing hybrid systems consisting of microgels covered with palladium nanoparticles. The P(NIPAM)-CS microgel system was synthesized first. For this, a solution of CS along with a small amount of acetic acid and deionized water (DW) was prepared in a beaker and stirred for 24 h. The mixture was then transferred to a flask and stirred (25 min) under N_2. The mixture was further stirred for 30 min in the presence of NIPAM at room temperature (26 °C) and then the temperature was raised to 70 °C. A small amount of APS solution was added to the reaction mixture for polymerization. Meanwhile, the Pd nanoparticles were synthesized in a separate beaker. Here, $PdCl_2$, trisodium citrate, and DW were added to a beaker and stirred. After 30 min, $NaBH_4$ solution was added to the beaker to reduce the Pd^{2+} ions.

This approach, however, is also not ideal for controlling the size of the nanoparticles and results in a wastage of nanoparticles in the medium. This method is applicable for core–shell (in which microgels are present as the core and metal nanoparticles as the shell) and homogenous hybrid microgels. Core–shell hybrid systems in which metal nanoparticles are present as the core and microgels as the shell cannot be synthesized by this method. Monometallic (Ag,[169] Cu,[164] Pd,[71] Au[96])-based hybrid systems have been synthesized using this method. Bimetallic (Pd,[167] Ag,[112] and Au[170]) nanoparticles-based hybrid microgels have also been reported using this approach. This method can also be used to synthesize bimetallic and other metal nanoparticle-based hybrid microgels.

4. Characterization techniques

Various techniques can be utilized to examine the size, structure, composition, behavior, and appearance of metal nanoparticle-based hybrid microgels, as well as to distinguish them from their corresponding smart microgels, as shown in Fig. 3(A)–(F). These techniques include scanning electron microscopy (SEM), wide-angle X-ray scattering (WAXS), polarizing optical microscopy (POM), energy-dispersive X-ray spectroscopy (EDX), dynamic light scattering (DLS), attenuated total reflectance spectroscopy (ATR), ^{1}H-nuclear magnetic resonance spectroscopy (NMR), laser light-scattering spectrometry (LLS), photoluminescence spectroscopy (PL), Raman spectroscopy (RS), UV-Visible spectrometry (UV-Vis), inductively coupled plasma mass spectrometry (ICP-MS), transmission electron microscopy (TEM), photo correlation spectroscopy (PSC), Fourier-transform infrared spectroscopy (FTIR), differential mechanical analysis (DMA), atomic force microscopy (AFM), inductively coupled plasma-optical emission spectrometry (ICP-OES), inductively coupled plasma atomic emission spectroscopy (ICP-AES), differential scanning calorimetry (DSC), and Brunauer–Emmett–Teller (BET) measurements.[171] Each characterization technique can provide specific information about both hybrid microgels and their corresponding microgels.

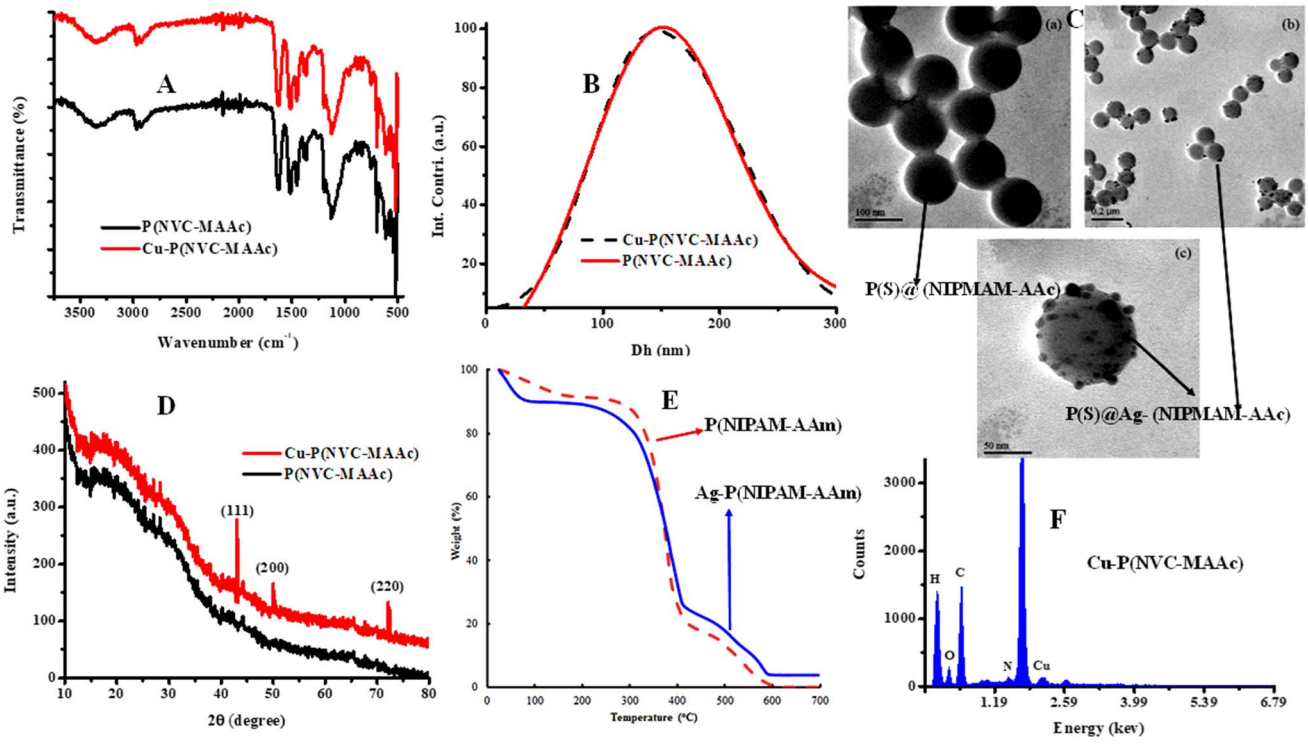

Fig. 3 Characterization techniques (A) FTIR, (B) DLS (reproduced from ref. 15 with permission from Elsevier, copyright 2023),[15], (C) TEM (reproduced from ref. 91 with permission from Elsevier, copyright 2019),[91], (D) XRD, (E) TGA (reproduced from ref. 151 with permission from Elsevier, copyright 2019),[151] and (F) EDX (reproduced from ref. 15 with permission from Elsevier, copyright 2023).[15]

Advanced microscopic techniques, like AFM, TEM, FE-SEM,[158] and SEM, can be employed to analyze microgel particles and their hybrids as well as their physical appearances. TEM can be used to investigate the size distribution, morphology, and size of both hybrid microgels and pure microgels, as shown in Fig. 3(C). It can provide information about the size and shape of polymer microgels and metal nanoparticles within the crosslinked polymer networks. SEM and AFM can be utilized to study the surface morphology of both metal nanoparticles and organic polymers.

FTIR (as shown in Fig. 3(A)), NMR,[172] and RS techniques are widely employed to investigate the functionalities of the resultant organic polymers and to identify interactions within the polymeric networks of microgels and metal nanoparticles in the form of hybrid microgels. EDX and XRD techniques can be used to verify the presence and properties of the metal nanoparticles in the crosslinked networks. XRD can also be used to determine the crystalline nature of both systems, as shown in Fig. 3(D). WAXS,[173] particle size analysis, and DLS (as shown in Fig. 3(B)) can be utilized to measure the diameter, size distribution, and size of particles. UV/Vis/NIR spectroscopy can be used to determine the volume phase transition temperature (VPTT) of both microgels and hybrid systems by measuring their turbidity. It can also be employed to confirm the stabilization and formation of plasmonic metal nanoparticles loaded in microgels. EDS can be used to find the elemental composites of the systems, as shown in Fig. 3(F).

TGA, DMA, and DSC[174] techniques can be employed to examine the thermal stability and decomposition of both microgels and hybrid systems. TGA can also be utilized to determine the content of metal nanoparticles in microgels, as shown in Fig. 3(E).[146] DLS/Photon correlation spectroscopy (PCS) can be applied to assess the size distribution and hydrodynamic sizes of microgels and hybrid microgels. WAXS can be employed to characterize the structure and consistency of the synthesized hydrogels, providing insights into the network topology, and ensuring reproducibility of the structures. Rheological measurements can be conducted to understand the viscoelastic properties of hydrogels.

Drug-release studies include evaluating the cytotoxicity of microgel and hybrid microgel systems using MTTS assays and quantifying the drug-release amount using the HP-LC[31]

Table 1 Hybrid microgels and their monomers, comonomers, metals, applications, and characterization techniques

System	Metal nanoparticles	Monomers	Applications	Characterization techniques	References
Ag-P(MAc), Co-P(MAc)	Ag, Co	MAc	Catalysis	FTIR, TEM, XRD, TGA, UV-Vis, EDX	146
Au-P(NIPr-AAc)	Au	NIPr, AAc	Colorimetric imaging	DLS, XPS, SEM, UV-Vis	174
Ag-P(NIPr-AAc-HEAc)	Ag	HEAc, NIPr, AAc	Drug delivery and biosensing	TEM, UV-Vis, XRD	177
Au/Cu-P(AN)	Au + Cu	AN	Catalysis	UV-Vis, TGA, FTIR, XPS, FE-SEM, EDX	158
Cu-P(AAc)	Cu	AAc	Catalysis	UV-Vis, TEM, WAXD, IR	173
Cu-P(AMPSAc), Co-P(AMPSAc), Ni-P(AMPSAc)	Cu, Co, Ni	AMPSAc	—	SEM, TEM, XRD, TGA, EDX	141
Pt-P(NIPr)	Pt	NIPr	Catalysis	TEM, ICP-AES, EDX, UV-Vis, DLS	130
Cu@Pd-P(NIPr-AAc)	Cu + Pd	AAc, NIPr	Catalysis	SEM, UV-Vis, XPS, XRD, FTIR, TEM, TGA	139
Cu-P(AAm-AAc)	Cu	AAm, AAc	Antibacterial	FTIR, UV-Vis, PS, SEM, XRD, DLS	178
Ag/Co-P(NIPMe)	Co + Ag	NIPMe	Catalysis	FTIR, XRD, UV-Vis, STEM, TGA	32
Ni-P(AAm-AAc)	Ni	AAm, AAc	Catalysis	XPS, FTIR, TGA, XRD, TEM	179
Mg/Pt-P(NIPr)	Pt + Mg	NIPr	Drug delivery	EDX, SEM, PL, CLSM	175
Ni-P(AAMPSA)	Ni	AAMPSA	Catalysis	TEM, ICP-AES, TGA	180
Au-P(NIPr-DMAEMA)	Au	DMAEMA, NIPr	Sensing	DLS, TEM, TGA, UV-Vis	72
Co-P(NipaM)/P(HemA)	Co	NIPAM, HEMA	Catalysis	TEM, ^{1}H NMR, FTIR, SEM, EDS, UV-Vis	172
Co-P(EI) poly(ethylene imine) P(EI)	Co	EI	Catalysis	FTIR, SEM, DLS, TGA, zeta potential	181
Ni/Ag-P(NIPMe-MAAc)	Ni + Ag	NIPMe, MAAc	Catalysis	FTIR, EDX, TGA, DLS, STEM, UV-Vis	61
Fe@Pd-P(NIPr-MMAc)	Fe + Pd	NIPr, MMAc	Catalysis	EDXS, ED-XRD, ICP-OES, DLS, SEM, FIB-SEM	176
Rh-P(NIPMe-AAc)	Rh	NIPMe, AAc	Catalysis	UV-Vis, XRD, FTIR	133
Pd-P(NIA-AA)	Pd	NIA, AA	Catalysis	FTIR, FE-SSEM, XRD, AFM, ICP-AES	182
Fe/Pd-P(AAc)	Fe + Pd	AAc	Catalysis	BET, ATR-FTIR, FE-SEM, XPS, ICP-AES, EDS	171
Ag/Pt-P(VA), Pt/In-P(VA), Pd/Fe-P(VA), Cu/Pd-P(VA), Pt/Fe-P(VA), Pt/Pd-P(VA)	Ag + Pt, Pt + In, Pd + Fe, Cu + Pd, Pt + Fe, Pt + Pd	VA	—	TEM, FTIR, SEM, UV-Vis, digital camera photography	140
sPd-P(NIA-MeAA)	Pd	NiA, MeAA	Catalysis	HP-LC, PCS, NMR, LC-MS	31

technique. Confocal laser scanning microscopy (CLSM)[175] can be utilized to monitor drug loading and release. ICP-OES,[176] ICP-MS, and ICP-AES[130] can be employed to determine the content of noble metal nanoparticles decorated by the microgels. Table 1 provides a summary of some microgels with metal nanoparticles, the characterization techniques used on them, and their applications.

5. Sensitivity properties

Microgels with and without metal nanoparticles both can show prompt responses to alterations in certain stimuli conditions, including pH,[183] ionic strength of a medium,[184] temperature,[185] and glucose level,[84] as shown in Fig. 4(a)–(f). These stimuli trigger abrupt changes in the hydrodynamic radius of the systems. The physical chemistry of this responsive behavior of these hybrid systems is explored in the following sections.

5.1. Temperature sensitivity

The change in hydrodynamic radius (HDR) of both microgels and hybrid microgels under different conditions of temperature is known as "temperature sensitivity". The temperature sensitivity of both systems can be assessed by monitoring the HDR relative to temperature changes, as shown in Fig. 4(a). The value of HDR can either decrease or increase with rising temperature, depending on the specific temperature-sensitive components in the microgel structure. Based on the temperature-sensitive components in hybrid microgel systems, their sensitivity can be classified as positive or negative temperature sensitivity.

Hybrid systems that swell at low temperatures and shrink at high temperatures are called negative-temperature-sensitive hybrid systems.[172,182,186–189] The temperature at which a sudden change occurs in the HDR of both microgels and hybrid microgels is known as the "Volume Phase Transition Temperature (VPTT)". Above this VPTT, the polymeric network is hydrophobic in nature. Therefore, water molecules can come into the crosslinked networks and expulsion takes place in these systems. The VPTT value can vary with alteration of the composition of the crosslinked polymer systems. This value is slightly higher in hybrid microgels than pure microgels, due to the occupation of some space by the metal nanoparticles in hybrid microgels, which slightly decreases the temperature sensitivity.[44]

The presence of MNPs makes it more challenging to heat these structures effectively, requiring a slightly higher temperature to remove water molecules from the polymer structure. Manikas *et al.*[190] reported that the VPTT of Au-P(NIPAM) hybrid microgels was higher than that of P(NIPAM) microgels. The temperature *versus* HDR curve shape for the hybrid systems closely resembled that of the original microgels, with a slight increase in the VPTT. Park *et al.*[174] studied the temperature-sensitive behavior of a core–shell system composed of gold nanoparticles as the core and poly(*N*-isopropylacrylamide-acrylic acid) P(NIPAM-AAc) as the shell. They showed that the VPTT could be adjusted by varying the acrylic acid (AAc) content. This adjustment was made to match with normal body temperature to aid drug delivery. Fernández-López *et al.*[188] described the development of Au-based hybrid microgels with longitudinal surface plasmon resonance in the near-infrared region. They achieved this by integrating Au nanorods into P(NIPAM) microgels, resulting in a photothermal effect triggered by the absorption of radiation in the water window region.

The positive temperature sensitivity of microgels and hybrid systems refers to their swelling behavior with the temperature increasing. In these systems, the moieties of the hybrid microgels/microgels are hydrophobic at low temperatures and hydrophilic at high temperatures. Consequently, the value of the HDR increases with increasing temperature.[139,191–193] Acrylamide-based systems typically exhibit a positive temperature sensitivity. These hybrid microgels also have an upper critical solution temperature (UCST), which is seldom reported in the literature. For example, Zhang *et al.*[192] synthesized Au nanorods loaded in hydrogels. These hybrid systems contained a triblock copolymer micelle with a poly(acrylamide-*co*-acrylonitrile) core and a poly(dimethylacrylamide) corona (water-soluble) at temperatures below the UCST. Upon exposure to near-infrared radiation, the gold nanorods absorbed light and converted it into heat. Therefore, the temperature of the medium would rise. This rise in temperature caused a transition in the solution by dissolving the micelles. Such a system shows potential as a light-triggered protein-delivery system.

Like temperature, laser light can also affect the swelling and deswelling behavior of hybrid microgels, as shown in Fig. 4(e). Such a swelling and deswelling behavior under laser light is more useful for drug delivery than others, and has been mostly used to date for drug delivery in cancer treatment.

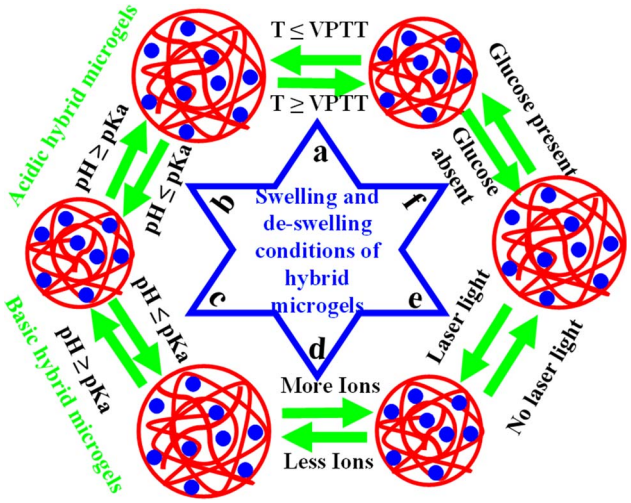

Fig. 4 Stimuli-responsive behaviors of hybrid microgels upon change in the (a) temperature, (b) pH of acidic hybrid microgels, (c) pH of basic hybrid microgels, (d) ionic strength of the medium, (e) laser light, and (f) glucose levels.

5.2. pH sensitivity

Hybrid systems are pH-sensitive because of the presence of acidic or basic components within the structures of the

crosslinked polymers. These components can undergo protonation or deprotonation by changing the pH of the medium. Due to the presence of acidic and basic components in the structure, hybrid systems can be categorized into three classes: (i) acidic hybrid microgels,[194] (ii) basic hybrid microgels,[195] and (ii) hybrid microgels with both acidic and basic natures.[196]

Hybrid systems that have acidic groups, such as –COOH[46,197,198] or $-SO_3H$,[63] in their structures are classified as acidic hybrid microgels. In these hybrid microgels, the HDR increases as the pH of the medium rises, as shown in Fig. 4(b). This behavior arises because these functional groups shift from an uncharged state to an anionic form as the pH of the medium increases (at pH $\geq$ pK_a). In the uncharged state, hydrogen bonding occurs due to the hydrogen being attached directly to a more electronegative atom (O). However, when protons are removed from these groups to form anionic species ($-COO^-$, $-SO_3^-$), electrostatic repulsion occurs between the anionic components due to their like charges. This conversion occurs when the pH of the solution exceeds the pK_a value. As a result of the increased hydrophilicity (electrostatic repulsion), water molecules diffuse rapidly into the crosslinked network. Conversely, these groups exist in the protonated (neutral) form (–COOH, $-SO_3H$) when the pH of the medium decreases (at pH $\leq$ pK_a).[74] In this condition, hydrophilicity (electrostatic repulsion) dominates. Thus, the HDR decreases with decreasing the pH of the medium and increases with increasing the pH of the medium. For example, Shah *et al.*[152] reported the pH responsiveness of gold nanoparticles in P(NIPAM-MAAc) microgels at room temperature in an aqueous medium. They observed that the HDR of the hybrid microgels increased with increasing the pH (pH = 2–6) due to the deprotonation of the –COOH groups of MAAc.

Hybrid microgels containing basic components, such as amino ($-NH_2$) groups, within their structure are called basic hybrid microgels. The amino groups are present in a neutral (deprotonated ($-NH_2$)) form at a high pH of the medium (p$K_a \geq$ pH), as shown in Fig. 4(c). In this scenario, amino groups form hydrogen bonding with other amino groups and with water molecules. However, at low pH (p$K_a \leq$ pH), the neutral amino groups are protonated into ammonium (cationic ($-NH_3^+$)) ions, leading to electrostatic repulsion between the ammonium ions and causing the hybrid microgels to swell.[98,132,199–203] Hydrogen bonding is present between the ammonium ions and water molecules, but electrostatic repulsion occurs between the ammonium ions themselves due to their like charges. Consequently, more water molecules can enter into the pores of the microgels in the cationic structure (protonated form, swelling state) compared to the neutral structure (deprotonated form, deswelling state). Tang *et al.*[72] conducted a study on the pH-sensitive properties of gold nanoparticles loaded in poly(*N*-isopropylacrylamide-2-(dimethylamino)ethylmethacrylate) P(NIPAM-DMAEMA) hybrid microgel systems at room temperature (25 °C) in an aqueous medium. They measured the HDR when varying the pH within the range of 3–9 and observed a gradual decrease in the values with increasing the pH from 3 to 9. This decrease was attributed to the amino groups shifting from a protonated form to a deprotonated form in the structure of the microgels. The presence of both DMAEMA and NIPAM functionalities within a single system made the system responsive to both pH and temperature variations.

Hybrid microgels that have both acidic (–COOH or $-SO_3H$) and basic ($-NH_2$) groups within their structures are called acidic/basic hybrid microgels.[71,204] Acidic/basic hybrid microgels exhibit swelling behavior upon decreasing or increasing the pH of the medium from the zero-charge-point (ZCP). The ZPC is the pH at which both acidic (–COOH or $-SO_3H$) and basic ($-NH_2$) groups have zero net charge. When the pH is reduced below the ZCP, the basic ($-NH_2$) groups become protonated, leading to repulsion among the components of the structures of hybrid systems, causing them to swell. While if the pH is greater than the ZCP, the acidic groups (–COOH or $-SO_3H$) undergo deprotonation, leading to electrostatic repulsion among the groups. In both these conditions, swelling occurs due to electrostatic repulsion and the HDR increases. While, at pH = ZCP, both the acidic and basic groups have zero net charge, and there is no electrostatic repulsion among the groups. There is thus no electrostatic repulsion, although hydrogen bonding is present. Therefore, the HDR decreases in this case compared to at other pH conditions. A pH-sensitive acidic/basic hybrid microgel system was reported by Zheng *et al.*[205] They studied the pH effect on the HDR of hybrid microgels at pH levels from 3 to 12. The maximum HDR value was observed at pH 8, attributed to electrostatic repulsion resulting from the negatively charged components. The HDR value reached a minimum at pH = 7, but started to increase once more as the pH was decreased further from 7 to 3, which could be attributed to protonation of the basic ($-NH_2$) groups. The pK_a and VPTT of some monomers and comonomers are given in Table 2.

5.3. Glucose sensitivity

Hybrid microgels that have phenyl-boronic acid in their structures and exhibit a swelling/deswelling behavior in the presence of glucose are called glucose-sensitive hybrid microgels, and their swelling and deswelling behavior is shown in Fig. 4(f). They are very important materials for the detection and quantification of glucose levels in blood samples.[206–208] During the detection, the –OH of boronic acid forms covalent bonds with the OH of glucose, leading to the reversible formation of ether. In the absence of glucose, the phenyl-boronic acid of the hybrid microgels exist in a dynamic equilibrium between the charged and uncharged forms in aqueous medium, as shown in Fig. 5. However, the presence of glucose shifts this equilibrium toward

Table 2 VPTT and pK_a values of different monomers and comonomers of hybrid microgels

Stimuli-responsive monomers/comonomers	Values of VPTT	Values of pK_a	References
NIPAM	32		190
NIPMAM	45		133
AAc		4.5	174
MAAc		5.5	152
AAMPSAc		2.3	63

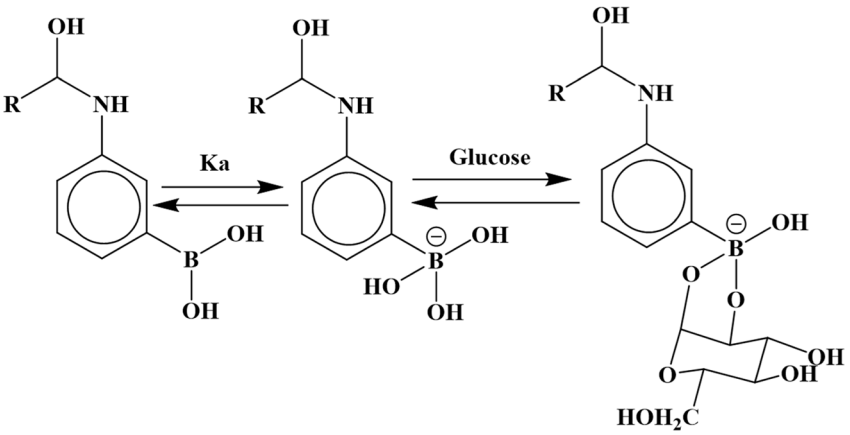

Fig. 5 Mechanism of glucose sensitivity.

the formation of a complex between the charged hybrid microgels and the components of the phenyl-boronic acid. Consequently, the charged content increases with a rising glucose concentration. Sensing using hybrid microgels has recently gained significant interest for optical glucose sensing. Zhang *et al.*[206] developed a Ag-based glucose-sensitive core–shell hybrid system, in which Ag nanoparticles served as the core and poly(3-acrylamidophenyl boronic acid-acrylic acid) P(AAPBAc-AAc) was the shell. When glucose interacts with AAPBAc, it increases the negative-charge density within the structure of the hybrid microgel. This leads to repulsive forces between the negatively charged functional groups, causing them to expand. In the absence of glucose, the size of the Ag-P(AAPBAc-AAc) hybrid microgels was reported to be 38 nm. However, as the concentration of glucose was increased from 0 mM to 30 mM, the size of the hybrid systems expanded from 38 nm to 53 nm. However, further increasing the glucose concentration did not result in a further size increase, as the hybrid microgels reached their maximum swelling limit. In this scenario, all the active sites (phenyl-boronic acids) of the hybrid microgels were bound with glucose. Ye *et al.*[84] developed glucose-sensitive Ag@poly(3-vinylaminophenylboronic acid-diethylaminoethyl acrylate) Ag@P(VAPBAc-DEAEAc) core–shell hybrid microgels, comprising silver nanoparticles at the core, with varying contents of DEAEAc (0.000501–0.0522 mol), which were used to explore the effect of the DEAEAc content on the glucose-sensitive behavior. At functional pH 7.4, the introduction of glucose to the hybrid microgels containing a high proportion of DEAEAc generated negatively charged boronated groups. These groups then formed bonds with the positively charged nitrogen of DEAEAc through electrostatic interactions, leading to a decrease in the HDR. A small quantity of DEAEAc could create negative charge upon exposure to glucose by its swelling behavior. While the pure microgels were not fluorescent, the hybrid microgels were so, even with the incorporation of a small number of nanoparticles. Basically, the physicochemical microenvironments around the Ag nanoparticles changes during the swelling/deswelling behavior. In other words, the refractive index of these hybrid microgels alters during their swelling/deswelling. Therefore, the optical property of Ag nanoparticles affected these hybrid microgels, but such optical property was not present in the pure microgels. Therefore, a change in photoluminescence (PL) intensity occurred when different concentrations of glucose were added during the investigation of glucose sensitivity due to the transformation from the swelling state to the deswelling state. The adsorption of glucose increased with increasing the content of DEAEAc, which decreased the PL intensity and *vice versa*. Zhang *et al.*[209] reported the glucose-sensitive behavior of Au-poly(*N*-isoproylacrylamide-3-acrylamidophenylboronic acid) Au-P(NIPAM-AAPBAc) hybrid microgels. They examined the swelling behavior of both the pure microgels and hybrid systems by varying the concentrations of glucose in the range of 0–30 mM. They observed a linear increase in the size of both systems with the increase in the concentration of glucose from 0 to 10 mM. However, no further increase in the size was observed upon further increasing the concentration of glucose from 10 to 30 mM, due to the unavailability of active sites (boronic acid groups) in the structures. These results suggested that boronic acid was an essential constituent of the structure for the detection and sensing of glucose.

5.4. Sensitivity to ionic strength

Hybrid microgels that show a swelling and deswelling behavior under various contents of ionic salts (metal salts) in a medium are called ionic strength-sensitive hybrid microgels, as shown in Fig. 4(d). The concentration of ionic salts affects the swelling and deswelling behavior of hybrid microgels.[170,210–213] When salts dissolve in a dispersion of hybrid microgels, they ionize due to the presence of water molecules. The structure of the hybrid microgels contains polar or ionic groups that interact with the produced ions. As a result, these ions penetrate the pores of hybrid microgels and decrease the diffusion rate of water molecules. This swelling/deswelling behavior depends on the nature of both the hybrid microgels and the salts. Das *et al.*[214] investigated the ionic-strength sensitivity of amphoteric silver-poly(*N*-isopropylacrylamide-*N*,*N*-dimethyl-*N*-(3-methacrylamidopropyl)-*N*-(3-sulfopropyl) ammonium betaine) Ag-P(NIPAM-DMSABe) hybrid microgels. These hybrid systems

showed a responsive behavior when a salt such as KCl or $CdCl_2$ was added to a dispersion of hybrid microgels. It was observed that the VPTT shifted to lower values as the salt concentration or oxidation state of the metal ions increased.

6. Applications

Hybrid microgels have potential and are already used in various applications in different fields, as shown in Fig. 6. A discussion about these applications is given below.

6.1. As an adsorbent

Microgels have polar components in their structures, which can interact with metal cations. Therefore, ions can penetrate into the crosslinked networks of microgels, where these ions are reduce into their corresponding atoms. However, these atoms are unstable, and thus they start to coagulate to obtain stability due to the atomic bonds. This coagulation is controlled by the crosslinked network as well as by stabilization of the particles.[126,215–217] In the presence of these metal nanoparticles, the structure of hybrid microgels also has an affinity to interact with other materials. In this way, the crosslinked network of hybrid microgels are responsible for this adsorption. Therefore, the adsorption of pollutants depends on the nature of the hybrid microgels (nature of the monomers, comonomers) and the nature of the adsorbents. More content will be absorbed if opposite charges are present on both the adsorbate and adsorbent.[66,76,77,138,218–223]

In this way selectivity can also be created in the hybrid microgel systems for the adsorption of specific pollutants, because the hybrid microgels will repel pollutants if the same charge is present on both. Mostly, the adsorption of pollutants by hybrid microgels is monitored by UV-Visible spectrophotometry (for all types of pollutants) or atomic adsorption spectrophotometry (only for metal ions). The adsorption of pollutants can be performed by mixing both the pollutants and hybrid microgels in an aqueous medium and stirring for some time. After that, the pollutant-loaded hybrid microgels are separated from the mixture by centrifugation or magnetic field (for magneto-sensitive hybrid microgels) and analyzed.[224]

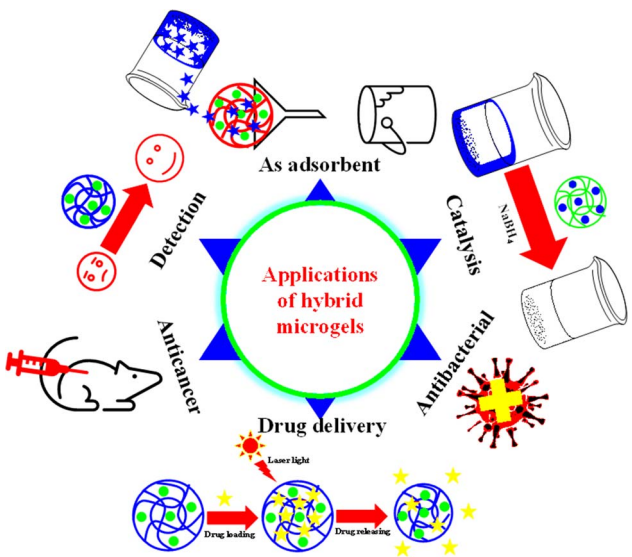

Fig. 6 Applications of hybrid microgels in different fields.

The sample pollutant solution before adding the hybrid microgel and after removing the hybrid microgels will be placed in a UV-Visible spectrophotometer or atomic adsorption spectrophotometer for analysis. The difference in the initial and final values indicates the removal percentage of pollutants. For example, Mizuno *et al.*[66] studied the adsorption of 4NiP by palladium nanoparticles-based hybrid microgels. The polar (–OH) functional groups in the hybrid microgels formed hydrogen bonds with the polar 4NiP. Therefore, 4NiP could be easily extracted by the crosslinked network of the hybrid microgels. Wang *et al.*[65] also used microgel systems to sorb palladium ions and simultaneously catalyze the reduction of 3NiP. The sorption of palladium ions occurred through ion–dipole interactions, followed by their reduction to palladium nanoparticles for the catalytic reduction of 3NiP. In this way, the metallic ion pollutants could be converted into metal nanoparticles, which are powerful catalysts for the reduction/degradation of pollutants.

6.2. Catalysis

The most important property of hybrid microgels is their catalytic behavior. They can be applied as catalysts for transformation/reduction/degradation reactions.[167,225–230] Hybrid microgels have several advantages over conventional catalytic systems, including:

(1) Nanoparticles have high stability within microgels due to the strong donor–acceptor interactions that are present between these nanoparticles and various functionalities of the microgels. These interactions can effectively prevent the leaching of MNPs from microgels during catalysis.[231,232]

(2) The porosity of hybrid microgels facilitates the approach of reactant molecules to the surface of MNPs.[233]

(3) The catalytic efficiency of hybrid microgels can be tuned by external stimuli, such as temperature,[185] ionic strength,[234] and pH.[183]

(4) The nanoparticles can be easily separated from the reaction product after completion of the reaction by centrifugation[32,51] or by applying a magnetic field.[96]

(5) The chemically inert nature of microgels ensures that they do not actively participate in the catalytic process.[43]

(6) In some instances, the polymeric network in hybrid microgels establishes a supportive environment that promotes the diffusion of reactant molecules from the bulk to the surface of metal nanoparticles, thereby enhancing the rate of the chemical reaction.

Various catalytic reactions can be done with hybrid microgels, with some common catalytic organic reactant conversions described below.

Hybrid microgels are frequently utilized as catalysts for the reduction of nitroarenes in aqueous media along with reducing agents like $NaBH_4$.[93,146,229,235–238] Four steps are involved in the catalytic reduction of nitroarenes, which can occur *via* either

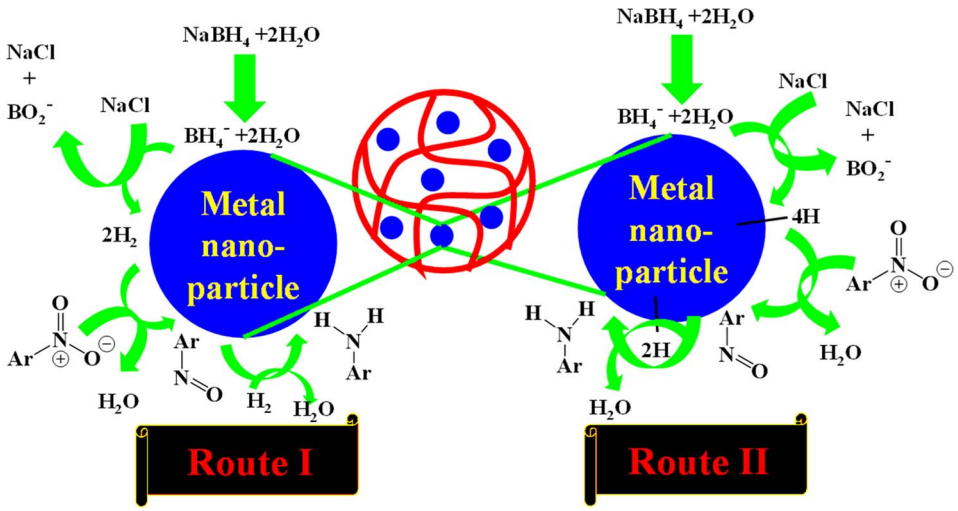

Fig. 7 Mechanism for the reduction of nitroarenes by hybrid microgels and $NaBH_4$.

route I or route II as shown in Fig. 7. Route II is preferred when the reaction proceeds rapidly, while route I is favored for slower reactions. In route I, H_2 gas is produced, which is highly stable and consequently less reactive; while nascent hydrogen is generated in route II that is extremely unstable and had high reactivity. As a result, the nascent hydrogen rapidly reacts with other molecules, leading to a faster product conversion, as depicted in route II.[43]

The catalytic reduction of 4NiP to 4-aminophenol (4AmP) is commonly employed as a model reaction to assess the catalytic efficiency of hybrid systems. This reaction was often selected due to the detoxification of 4NiP into the less toxic 4AmP, which can further be converted into various organic compounds. Another reason is the easy monitoring of the 4NiP reduction process. The progression of the reduction reaction can be monitored using a UV/Vis spectrophotometer, where a decrease in the absorbance at 400 nm and the appearance of a new peak around 300 nm indicate the conversion of 4NiP to 4AmP. Similar trends in absorbance have been reported by Aldabergenov *et al.*,[239] Ulker *et al.*,[240] and Tatykhanova *et al.*[241]

Numerous factors influence the catalytic efficiency of hybrid systems during the reductive reduction of nitroarenes, as shown in Fig. 8(A)–(C). The quantity of metal nanoparticles present in the hybrid microgels is a key factor determining the reduction rate,[63,82] whereby increasing their content in hybrid systems enhances the reduction rate of nitroarenes. Gancheva and Virgilio[241] synthesized both porous and non-porous microgels loaded with different amounts of Au nanoparticles. The

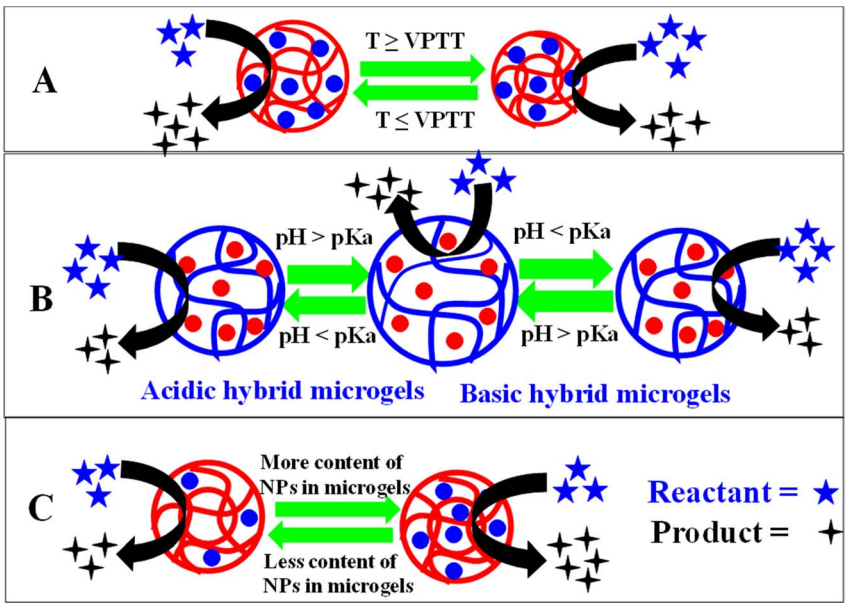

Fig. 8 Catalytic reduction of nitroarenes by hybrid microgels under different (A) temperatures, (B) pH levels of the medium, and (C) contents of metal nanoparticles in the microgels.

catalytic activity of the porous hybrid systems with a greater content of Au NPs (2.7 wt%) surpassed that of the non-porous systems. Similarly, Zhou *et al.*[128] investigated the effect of the content of MNPs on the catalytic reductive reactions and reported similar catalytic trends.

The catalytic efficiency can be tuned by varying the temperature, as shown in Fig. 8(A). The temperature dependence deviates from t normal Arrhenius behavior in the case of temperature-sensitive hybrid microgels. The HDR of hybrid microgels decreases as the temperature of the medium rises. The HDR exhibits its maximum derivative at the VPTT. Below the VPTT, the hydrogels are present in a swelling state, allowing reactant molecules to easily access the MNPs surface; therefore facilitating a rapid conversion of the reactants to products. Conversely, the catalytic reductive reaction rate decreases at temperatures above the VPTT due to the shrinkage and the resulting decrease in the HDR. This shrinkage makes it more challenging for reactants to reach the catalyst surface.[57,74,75,242] The use of the Arrhenius equation provides a quantitative method to analyze the temperature impact on the reaction rate catalyzed by hybrid systems. The relationship between the natural logarithm of the reaction rate constant ($\ln k_{app}$) and the reciprocal of temperature ($1/T$) within the temperature range encompassing the VPTT has been observed to be non-linear. Further, it has been found that the k_{app} value increases with temperature, reaches a minimum at the VPTT, and then starts to rise again. The temperature effect on the k_{app} value for the catalytic reductive reaction of 4NiP in the presence of hybrid microgels and $NaBH_4$ was investigated by Hussain *et al.*[243] and Rehman *et al.*[152]

The catalytic efficiency of hybrid microgels can readily be controlled by adjusting the pH of the medium during the catalytic reductive reactions, as shown in Fig. 8(B). This pH sensitivity is present if the structures of the hybrid microgels have basic ($-NH_2$)[244] or acidic (–COOH,[46,245], $-SO_3H$[63]) groups. The pH effect on these acidic (–COOH, $-SO_3H$) and basic ($-NH_2$) groups is opposite in nature, as one group ($-NH_2$) is basic in nature while the other (–COOH, or $-SO_3H$) is acidic. Acidic hybrid microgels have –COOH or $-SO_3H$ groups in their structure. These groups exhibit a swelling behavior when the pH of the medium increases above the pK_a value. Once the pH exceeds the pK_a value of the ionic portion, all the acidic ($-SO_3H$ or –COOH) groups will convert into anions ($-SO_3^-$ or $-COO^-$). These negatively charged groups repel each other electrostatically, leading to an increase in the HDR. In this swollen state, a greater number of reactant species can easily access the MNPs surface, resulting in a higher conversion of reactants into products, together with an increased apparent rate constant. In contrast, at pH values $\leq$ pK_a, the hybrid microgels undergo deswelling, limiting the number of reactants that cab reach the MNPs surface and consequently yielding a smaller amount of product. Shah *et al.*[152] investigated the impact of pH on the catalytic efficiency. They noted that at pH 2.78, the k_{app} value was 0.196 min^{-1}, which increased to 0.321 min^{-1} at pH 8.36. Additionally, they observed that higher concentrations of monomers containing acidic groups resulted in an improved catalytic performance, likely due to the greater swelling.

The catalytic performance can be impacted by the presence of basic ($-NH_2$) groups in the hybrid microgel structure, which can be regulated by adjusting the pH of the medium, as shown in Fig. 8(B). At low pH values, the basic ($-NH_2$) groups exist in a protonated ($-NH_3^+$) form, leading to electrostatic repulsion caused by the cationic functionalities within the structure. As a result, the HDR value is lowered at high pH and increases with decreasing the pH value. Tan *et al.*[93] studied the catalytic activity for the reduction of 4NiP over a pH range of 3 to 11. They observed that the value of k_{app} was highest at pH 3 and gradually declined as the pH increased. For example, at room temperature, the k_{app} value was 7.3×10^{-3} s^{-1} at pH 3 and 7.4×10^{-4} s^{-1} at pH 7.

The catalytic efficiency of bimetallic nanoparticles-containing hybrid systems exceeds that of monometallic nanoparticles systems for the reduction of nitroarenes.[94,146,163] The addition of metallic nanoparticles to systems containing other metallic nanoparticles can enhance each other's performance due to a synergistic effect. The interface formed between one type of MNPs and another type of MNPs in the hybrid microgels enhances the catalytic performance. The work function values of both types of MNPs play a role in creating a depletion region, causing electron transfer from the lower work function side to the higher work function side. This interaction between electron-deficient reactants (nitroarenes) and electron-rich nanoparticles allows a greater number of reactant molecules to reach the nanoparticles' surface, resulting in a faster reduction reaction.[246] Li *et al.*[82] reported the synthesis of bimetallic (Ag + Au) hybrid microgels. They loaded gold NPs with varying concentrations in Ag-based hybrid microgels and observed that the k_{app} value for the catalytic reductive reaction of 4NiP in the presence of each hybrid system increased with increasing the amount of Au NPs. Similarly, Tan *et al.*[93] investigated the catalytic activity of a bimetallic (Au + Ag) hybrid system in which Ag nanoparticles were loaded into Au-based hybrid microgels.

The content of the reductant ($NaBH_4$) and the content of metal nanoparticles in the microgels (as shown in Fig. 8(C)) also impacted the catalytic efficiency;[43,61,115] whereby a higher reductant concentration increased the k_{app} value, leading to a faster completion of the reaction. Essentially, the higher reductant content resulted in more of the compound being adsorbed onto the catalyst surface, leading to increased hydrogen release, which in turn affected the rate of product formation. Hussain *et al.*[243] studied the catalytic performance of Ag nanoparticle-encapsulated core–shell microgel systems under various $NaBH_4$ concentrations and noted that the reaction rate increased with higher $NaBH_4$ concentrations.

The number of nitro groups in nitroarenes also influences the catalytic performance of hybrid microgels. Therefore, the k_{app} value for the reduction of tri-nitroarenes is smaller than that for mono-nitroarenes under similar conditions. Mono-nitroarenes can thus be reduced more rapidly compared to di- and tri-nitroarenes. Melinte *et al.*[247] investigated the catalytic reduction of 2,6-dinitrophenol (di-nitroarene), 4NPh (mono-nitroarene), and picric acid (tri-nitroarene) under similar conditions and calculated the k_{app} values for each reductive

reaction as 16.52×10^{-3}, 34.35×10^{-3}, and 12.31×10^{-3} min^{-1}, respectively.

The rate of reduction can be significantly influenced by the presence of specific gases dissolved in the aqueous dispersion of the reaction mixture. The catalytic performance of hybrid microgels is different in N_2 and CO_2 gaseous environments. CO_2 gas purging in hybrid microgel dispersions leads to the transformation of carboxylic (–COOH) groups, which thus alters the interfacial interactions between the functionalities of the microgels and MNPs. Thus, the catalytic activity can be significantly affected by purging with CO_2. In one study,[44] the impact of introducing N_2 and CO_2 gases into the reaction mixture was examined in relation to the catalytic efficiency of Au-P(NIPAM-MAAc) for 4NiP reduction. It was found that the k_{app} values were 2.1×10^3 and 3.2×10^3 min^{-1} for N_2 and CO_2 gas purging, respectively, at $T \leq 29$ °C. At $T \geq 35$ °C, the k_{app} values were 1.3×10^4 and 1.4×10^{12} min^{-1} for N_2 and CO_2 purging, respectively.

The reduction rate of nitroarenes also depends on the substituent and position of the attached substituent on the nitro-benzene ring.[43,58,151,248] If the substituent is an electron-donating species, then the reduction rate is low; while if an electron-withdrawing group is attached directly to the ring, then reduction can rapidly take place.[43] Basically, nitro groups are electron deficient, and their deficiency can be reduced by electrons provided by the metal nanoparticles. If the electron-donating group is directly attached to the ring, it donates some electronic cloud to the nitro group. Therefore, the electron deficiency is minimized by electron-donating groups, and their capacity to obtain electrons from metal nanoparticles is also reduced, resulting in reduction rated. On the other hand, an electron-withdrawing group would further decrease the electronic cloud from the ring. Therefore, rings do not donate their electronic cloud to nitro groups. Therefore, they rapidly gain electrons from MNPs and reduce them rapidly.

Dyes are a major source of water pollution, and are used in textile industries on a large scale. These industries discharge these dyes as waste material. These dyes are very toxic to human health. Therefore, it is a very important task to remove these dyes from contaminated water. To address this problem, various catalytic systems are used to degrade or reduce the toxic dyes into harmless compounds. Hybrid microgels are considered the best materials for rapid catalytic reduction or degradation.[14,67,139,215,216,249] Shah *et al.*[250] investigated the catalytic performance of Au- or Ag-based hybrid microgels for the reduction of Congo red (CR), 4-nitrophenol (4NiP), and methylene blue (MB). They showed excellent results for industrial wastewater treatment. Their catalytic efficiency in wastewater was slightly lower than pure water, due to the presence of various metallic and nonmetallic ions in wastewater, which interact with the polar components of hybrid microgels and resist the approach of dyes to the surface of MNPs. Han *et al.*[251] studied the catalytic performance of Au-based hybrid microgels for the reduction of MB, rhodamine B (RAB), and 4NiP. They observed that 4NiP and organic dyes were adsorbed onto the Au nanoparticle surface and then desorbed as products. The catalytic efficiency of the hybrid system followed the order: MB > RAB > 4NiP. Similarly, Cao *et al.*[252] investigated the catalytic activity of gold nanoparticles encapsulated in core–shell hybrid systems for the reduction of 4NiP and RAB. They found there was no significant decrease in the catalytic performance of the hybrid systems after recycling.

Hybrid microgels show excellent catalytic performance for coupling reactions conducted under various conditions. Increasing the temperature can enhance the reaction rate, leading to the formation of more products in a shorter time. With higher temperature, a greater fraction of reactant molecules have kinetic energy (KE) equal to or greater than the activation energy (E_a), resulting in more collisions and a higher reaction rate. The choice of solvent also affects the catalytic efficiency of hybrid microgel systems in coupling reactions. Among the organic solvents, ethanol has been found to be the most effective. Eyimegwu *et al.*[253] utilized hybrid microgels for various homocoupling reactions under different solvents in aerobic conditions. Albino *et al.*,[254] Wang *et al.*,[65] and Hong *et al.*[255] investigated coupling reactions in the presence of Pd nanoparticle-decorated microgels. Pourjavadi *et al.*[256] used core–shell hybrid microgels for the reduction of 4NiP and for Suzuki–Miyaura coupling reactions. They conducted coupling reactions between substituted iodo/bromobenzenes and phenyl-boronic acid under different solvents, temperatures, and bases, and found that a higher product yield was obtained in water compared to in other solvents under similar conditions. Additionally, they noted that the presence of an electron-withdrawing group attached to the iodo-/bromobenzene resulted in a higher yield, whereas the presence of an electron-donating group led to a lower yield.

6.3. Detection

Hybrid microgels show excellent performance for the detection (sensing) of various materials, like toxic metal ions in water.[184,257–259] Tang *et al.*[72] explored the sensing properties of gold nanoparticles incorporated into poly(*N*-isopropylacrylamide-2-(dimethylamino)ethylmetharylate) P(NIPAM-DMAEMA) for the detection of Hg^{2+} ions. They observed a linear relationship between the fluorescence intensity and the concentration of mercuric ions after adding a mercuric ions solution in to a dispersion of 1-pyrenebutyric acid (PBA) containing hybrid microgels. This behavior was attributed to replacing the PBAc with Hg^{2+} ions from the hybrid microgels. As the concentration of Hg^{2+} ions increased from 0.16 to 1.60 μM, there was an increase in the fluorescence intensity, which could be used to accurately quantify the Hg^{2+} ions in the samples. Similar experiments were conducted under similar conditions with other metal ions. The results showed that metals other than Hg^{2+} did not induce significant changes in the fluorescence intensity. This indicated that the hybrid microgels could be used selectively for sensing Hg^{2+} ions.

Hybrid microgels can also help in detecting thrombin, which is an enzyme responsible for converting fibrinogen into fibrin in the human body. Gui *et al.*[73] devised an electrochemiluminescent aptasensor by combining a ruthenium (Ru) complex with hybrid microgels to sense thrombin using an

electro-generated chemiluminescence method. Upon adding thrombin to the hybrid microgels containing Ru, the peak intensity increased. This peak intensity exhibited a direct correlation with the concentration of thrombin, spanning from 1.0 fM to 10 pM, with a detection limit of 0.54 fM.

Different substances can also be detected by hybrid microgels. The sensing/detection abilities of the hybrid microgels are usually evaluated using cyclic voltammetry, which is a technique that tracks the oxidation and reduction positions of the sensor. The sensing ability is determined by observing any shift in the oxidation or reduction potential of the sensor in the presence of a specific substance, enabling the detection of even minute quantities of substances. Mutharani *et al.*[71] investigated the detection of organophosphorus pesticide paraoxon-ethyl by using hybrid microgels at various concentrations (0.01 μM to 1.3 mM), and demonstrated remarkable results. Tang *et al.*[260] studied the sensing ability of Pd-P(AAc) for H_2O_2. They observed a reduction peak at 0.1 V for H_2O_2. A similar reduction peak was obtained with Au/Pd^{2+}-P(AAc), albeit with a significantly lower intensity. However, no such reduction peak was observed with Au/P(AAc) in the presence of H_2O_2.

6.4. Drug delivery

Smart microgels with metal nanoparticles have attracted significant attention as drug-delivery systems owing to their sensitivity under different pH, temperature, and electromagnetic radiation conditions.[132,261–266] These hybrid systems can be used for the delivery of drugs into the body, as shown in Fig. 9. Upon reaching the target site, laser light (in the water window or near-infrared spectrum) is applied and directed toward the designated area. Au-based hybrid systems can absorb the light and convert it into heat energy, which increases the temperature. This temperature rise triggers a phase transition in the hybrid microgels, facilitating the release of the drug at the targeted location. Solorzano *et al.*[266] conducted a study on a photoresponsive drug-delivery system utilizing hollow gold nanoparticles-incorporated P(NIPAM) systems. The hybrid microgels were loaded with bupivacaine hydrochloride monohydrate drug. The researchers investigated the drug-release kinetics under near-infrared irradiation, and demonstrated the potential of the Au-P(NIPAM) hybrid system as a promising photothermally triggered drug carrier.

The loading and release of a drug may be studied in different pH conditions. Hybrid microgels show a swelling and deswelling behavior in different pH conditions and it is this swelling and deswelling behavior that control the loading and release of the drug. In this way, the pH of the medium is also an important parameter for drug-delivery systems. The controlled release behavior of hybrid microgels can be obtained by adjusting the content of monomers, comonomers, and crosslinkers during the formation of hybrid microgels. The naturalness of the monomers, comonomers, and crosslinkers is also an important aspect for drug delivery. They also have an effect on loading and release of the drug in the systems through variations in the polarity. Therefore, the interactions that occur between the drug and structure of the hybrid microgels during the loading and release of the drug depend on the nature of both the hybrid microgels and the drug.

6.5. Anticancer/antitumor treatment

Hybrid microgels can be used in tumor/cancer treatment.[47,267–269] For these applications, both the MNPs and the organic components of hybrid systems play pivotal roles in cancer therapy. Specifically, Au nanoparticles possess the ability to absorb light within the wavelength range of 500–1200 nm and convert this absorbed light into thermal energy through a radiation-less relaxation process. Consequently, the temperature of the local environment increases when near-infrared light is applied at the target area of the body after the injection of hybrid microgels. This rise in temperature facilitates tumor treatment through a photothermal mechanism. Wang *et al.*[270] developed Au-based gelatin for photothermal therapy. This hybrid system demonstrated notable characteristics, like excellent stability, a high content of Au NPs, and low degradability, making it suitable for effective photothermal therapy.

The combination of photothermal therapy and chemotherapy presents a favorable approach for cancer treatment with high potential efficiency. The temperature sensitivity of hybrid microgel systems plays a critical role in controlling the release of loaded anticancer drugs, as discussed earlier. Zhou *et al.*[68] developed a hybrid microgels system and used this for the loading and release of the anti-inflammatory drug diclofenac sodium (DS) and the anticancer drug doxorubicin (DR). The gold nanoparticles in the hybrid microgel served several functions: they can absorb DR on their surface, which can then be

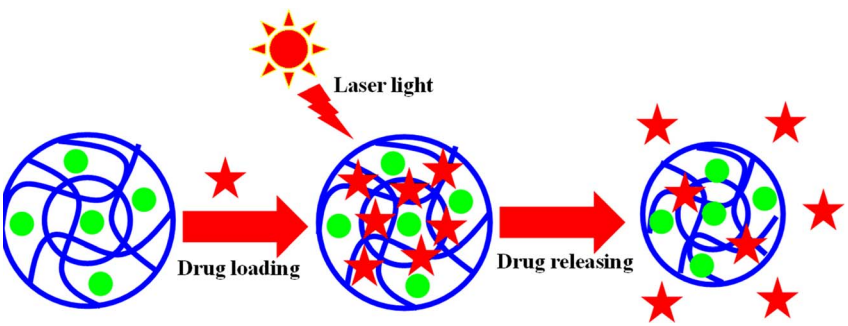

Fig. 9 Loading and release of a drug by hybrid microgels.

replaced by glutathione (GT) present within tumor cells, and they have the ability to convert absorbed light into heat, triggering a volume phase transition in the microgels, resulting in the release of the DS.

6.6. Antibacterial activities

Hybrid microgels exhibit excellent antibacterial properties by releasing metal ions into an aqueous medium through a porous microgel system, surpassing the antibacterial efficiency of bulk metals. Unlike toxic agents, metal nanoparticles demonstrate antibacterial activity without releasing harmful substances.[70,122,125,226,271,272] By penetrating bacterial membranes, Ag^+ ions have the ability to replace various other metal cations, such as Ca^{2+}, in biological systems.[273] Additionally, they can attach to electron-donating groups, like carboxylate, phosphate, and thiol groups, present in DNA. They can interrupt normal cellular processes, leading to the death of bacterial cells.[274] Consequently, they are effective at eradicating bacteria such as *Staphylococcus epidermidis* (*S. epidermidis*),[214] *Staphylococcus aureus* (*S. aureus*),[275–277] *Pseudomonas aeruginosa* (*P. aeruginosa*),[276,278] and *Escherichia coli* (*E. coli*).[70,122,271,279–281] For example, Hantzschel *et al.*[276] examined the antibacterial activity of Ag-based hybrid microgels by observing the growth of bacterial colonies of *S. aureus* and *P. aeruginosa* over time with varying the content of Ag NPs in the hybrid microgels. They observed there was a notable reduction in bacterial growth, and the antibacterial activity was enhanced with increasing the Ag NPs content. Microgels containing 11.2% Ag nanoparticles exhibited more effective antibacterial properties against *P. aeruginosa* compared to *S. aureus*. This difference was attributed to the thinner murein layer of *P. aeruginosa* compared to *S. aureus*, allowing for a faster diffusion rate of the antibacterial agent into the bacterial cells, resulting in a quicker eradication. The researchers demonstrated that as the content of Ag nanoparticles increased, the antibacterial effectiveness of the hybrid microgels also increased. In a separate study, Thomas *et al.*[282] investigated the antibacterial activity of hybrid systems against *E. coli*. They examined the effects of the hybrid microgel particle size, Ag NPs loading, and the content of AAc present in the hybrid systems on the antibacterial activities of the hybrid microgel. They found that hybrid systems with a size of 100 μm showed a superior inhibition of bacterial colony growth compared to those with a size of 200 μm in an aqueous medium due to the reduction in the surface area of larger particles. The antibacterial performance against *E. coli* increased with a higher content of Ag NPs within the microgels. The study highlighted that the feed composition of the microgels significantly influenced their antibacterial properties, with hybrid systems containing 5.55 mM of AAc demonstrating greater efficiency compared to those with no AAc content (0.00 mM AAc).

7. Conclusion and future directions

The integration of metal nanoparticles into smart microgels creates unique and intriguing hybrid systems. These hybrids exhibit responsive behaviors, leading to a diverse range of hybrid microgels with distinct shapes, compositions, and structures. These systems have demonstrated remarkable performance in catalytic reactions and their performance can be controlled by varying their size and morphology. Consequently, these systems are predominantly used in catalytic reactions over other applications. Their catalytic efficiency can be tuned with external stimuli conditions, like pH, temperature, solvent nature, and ionic strength of the medium. Moreover, the potential applications of hybrid microgels in various fields, such as drug delivery, adsorption, antibacterial, and anticancer, are influenced by their morphology, which can be customized to specific requirements using suitable synthetic techniques. The morphologies, functional hierarchy, and crystallinity of synthesized hybrid systems can be identified using diverse characterization techniques.

Some metal ions (like palladium ions) exhibit significant environmental toxicity, limiting their direct applicability. However, these ions can be converted into valuable substances, as demonstrated by their incorporation in nanocomposites such as palladium nanoparticle-based hybrid microgels. These composite materials with palladium nanoparticles present in the microgels have diverse applications across various fields. However, the toxicity of palladium metal hinders the use of palladium-based hybrid microgels in drug-delivery applications, highlighting a notable drawback of these hybrid microgels.

Another drawback observed in previously reported hybrid microgels is the use of non-biodegradable monomers during their synthesis. For instance, *N*-isopropylacrylamide has been widely utilized in the synthesis of hybrid systems, but leads to the formation of non-biodegradable microgels. This limitation could be addressed by employing biodegradable monomers, like *N*-vinyl caprolactam. Metal nanoparticle-decorated microgels have shown the best performance involving catalyst transformation for specific organic reactions, notably in the reduction of 4-nitrophenol. Thus, investigating the catalytic potential of hybrid microgels across a range of organic transformations could provide valuable insights for future research. Bimetallic nanoparticles-containing hybrid microgels have demonstrated significantly enhanced performance for many catalytic reduction and degradation reactions compared to monometallic hybrid systems. Therefore, a more comprehensive examination of bimetallic hybrid systems is warranted. Moreover, the high cost of noble metals, excluding palladium (which is toxic), presents a challenge that can be addressed by combining these metals with less expensive ones in bimetallic hybrid systems. Additionally, recycling hybrid systems after catalysis offers a potential solution to this challenge. Further research is needed to explore the leaching effect and catalytic performance of recycled hybrid microgels. Moreover, the factors directly influencing the catalytic efficiency of bimetallic hybrid microgels, such as temperature, solvent nature, pH levels, and ionic strength of the medium, require thorough exploration in future studies. Furthermore, forthcoming research should evaluate the compatibility of hybrid polymers with various substrates to assess their potential applications.

Metal nanoparticles have found expanded applications within microgels, which can contain both polar and non-polar components in their structure. Consequently, hybrid microgels present potential uses in catalysis (noble metal nanoparticles) as well as in adsorption processes (microgel component). Although only a few hybrid microgel systems have been employed in adsorption processes thus far, there is an opportunity to explore these as alternative systems for the removal of various water pollutants, including heavy metal ions and harmful organic dyes. These hybrid systems may prove to be the best option for the purification of industrial wastes through a combination of adsorption and catalytic reactions.

Abbreviations

AAc	Acrylic acid
AAm	Acrylamide
NIPMAM	*N*-Isopropylmethacrylamide
NIPAM	*N*-Isopropylacrylamide
NPs	Nanoparticles
SMGs	Smart microgels
MAAc	Methacrylic acid
MNPs	Metal nanoparticles
MB	Methylene blue
CR	Congo red
4NiP	4-Nitrophenol
4AmP	4-Aminophenol
DMAEMA	2-(Dimethylamino)ethylmethacrylate
VCL	*N*-Vinylcaprolactam
AAEMA	Acetoacetoxyethylmethacrylate
MCMCS	Maleate carboxylmeth chitosan
EA	Ether amine
AAMPSAc	2-Acrylamido-2-methylpropane sulfonic acid
DLS	Dynamic light scattering
SDS	Sodium dodecyl sulfate
MO	Methyl orange
RAB	Rhodamine B
PBAc	1-Pyrenebutyric acid
DS	Diclofenac sodium
DRC	Doxorubicin
GT	Glutathione
EDX	Energy-dispersive X-ray spectroscopy
FTIR	Fourier-transform infrared spectroscopy
HDR	Hydrodynamic radius
HRTEM	High-resolution transmission electron microscopy
LCST	Lower critical solution temperature
MIEEMACh	2-(1-Methylimidazolium-3-ethyl)-ethyl methacrylate chloride
MMAAc	Methylmethacrylic acid
MBAAm	*N*,*N*′-Methylene-bisacrylamide
APS	Ammonium persulfate
MAPTMSi	3-Methacryloxypropyltrimethoxy silan
GR	Galvanic reaction
HEA	2-Hydroxyethyacrylate
VP	4-Vinylpyridine
SEM	Scanning electron microscopy
SPR	Surface plasmon resonance
TGA	Thermogravimetric analysis
DEAEAc	Diethylaminoethylacrylate
UV-Vis	UV-Visible spectroscopy
VPTT	Volume phase transition temperature
XPS	X-ray photoelectron spectroscopy
XRD	X-ray diffraction
P(EI)	Poly(ethyleneimine)
AAPBAc	3-Acrylamidophenyl boronic acid
VA	Vinyl alcohol
VAPBAc	3-Vinylaminophenyl boronic acid
ICP-AES	Inductively coupled plasma atomic emission spectroscopy

Data availability

Data will be provided on request.

Conflicts of interest

There are no conflicts of interest to declare.

Acknowledgements

Muhammad Arif is thankful to University of Management and Technology, Lahore 54770, Pakistan.

References

1 A. Ben Ali, R. Elaf, M. Saad, I. A. Hussein and B. Bai, *Emergent Mater.*, 2023, 1–11.
2 M. Arif, A. Rauf and T. Akhter, *Int. J. Biol. Macromol.*, 2024, **274**, 133250.
3 M. Arif, *Eur. Polym. J.*, 2024, **206**, 112803.
4 N. Hazra, A. Ninarello, A. Scotti, J. E. Houston, P. Mota-Santiago, E. Zaccarelli and J. J. Crassous, *Macromolecules*, 2024, **57**, 339–355.
5 M. Arif, H. Raza, S. M. Haroon, S. Ben Moussa, F. Tahir and A. Y. A. Alzahrani, *Int. J. Biol. Macromol.*, 2024, **270**, 132331.
6 M. Arif, *J. Mol. Liq.*, 2024, **403**, 124869.
7 M. Arif, *RSC Adv.*, 2024, **14**, 9445–9471.
8 G. Agrawal and R. Agrawal, *Small*, 2018, **14**, 1801724.
9 M. Arif, *JOM*, 2024, **76**, 1203–1222.
10 M. Arif, *Polymers*, 2023, **15**, 3600.
11 D. C. Leite, S. Kakorin, Y. Hertle, T. Hellweg and N. P. da Silveira, *Langmuir*, 2018, **34**, 10943–10954.
12 M. Arif, A. Rauf, H. Raza, S. B. Moussa, S. M. Haroon, A. Y. A. Alzahrani and T. Akhter, *Int. J. Biol. Macromol.*, 2024, **275**, 133633.
13 V. Sabadasch, M. Dirksen, P. Fandrich and T. Hellweg, *Front. Chem.*, 2022, **10**, 889521.
14 M. Shahid, Z. H. Farooqi, R. Begum, M. Arif, W. Wu and A. Irfan, *Crit. Rev. Anal. Chem.*, 2020, **50**, 513–537.
15 M. Arif, H. Raza, S. M. Haroon, K. Naseem, H. Majeed, F. Tahir, U. Fatima, S. M. Ibrahim and S. Ul Mahmood, *J. Mol. Liq.*, 2023, **392**, 123541.

16 M. Shahid, Z. H. Farooqi, R. Begum, M. Arif, A. Irfan and M. Azam, *Chem. Phys. Lett.*, 2020, **754**, 137645.
17 M. Dirksen, T. A. Kinder, T. Brändel and T. Hellweg, *Molecules*, 2021, **26**, 3181.
18 M. Dirksen, C. Dargel, L. Meier, T. Brändel and T. Hellweg, *Colloid Polym. Sci.*, 2020, **298**, 505–518.
19 X. Li, L. Hetjens, N. Wolter, H. Li, X. Shi and A. Pich, *J. Adv. Res.*, 2023, **43**, 87–96.
20 M. Marquis, D. Musino, V. Gemin, L. Kolypczuk, D. Passerini and I. Capron, *Carbohydr. Polym. Technol. Appl.*, 2023, **6**, 100405.
21 L. Liu, Y. Liu, H. Zhong, X. Li, Y. Jun, Q. Wang, L. Ding, Z. Cheng and H. Qian, *Colloids Surf., B*, 2023, **229**, 113432.
22 M. Arif, A. Rauf and T. Akhter, *RSC Adv.*, 2024, **14**, 19381–19399.
23 M. Tang, Y. Sun, X. Feng, L. Ma, H. Dai, Y. Fu and Y. Zhang, *Food Chem.*, 2023, **419**, 136044.
24 X. Wan, Q. Kang, J. Li, M. Guo, P. Li, H. Shi, X. Zhang, Z. Liu and G. Xia, *Food Chem.*, 2024, **433**, 137395.
25 D. E. Demco and A. Pich, *Macromol. Chem. Phys.*, 2023, **224**, 2200410.
26 T. Nevolianis, A. Scotti, A. V. Petrunin, W. Richtering and K. Leonhard, *Polym. Chem.*, 2023, **14**, 1447–1455.
27 M. Arif, *Z. Phys. Chem.*, 2023, **237**, 809–843.
28 S. K. Wypysek, S. P. Centeno, T. Gronemann, D. Wöll and W. Richtering, *Macromol. Biosci.*, 2023, **23**, 2200456.
29 H. P. Lim, S. S. D. Ng, D. B. Dasa, S. A. Adnan, B. T. Tey, E. S. Chan, K. W. Ho and C. W. Ooi, *Int. J. Biol. Macromol.*, 2023, **232**, 123461.
30 M. Arif, *J. Environ. Chem. Eng.*, 2023, **11**, 109270.
31 V. Sabadasch, S. Dachwitz, Y. Hannappel, T. Hellweg and N. Sewald, *Synthesis*, 2022, **54**, 3180–3192.
32 M. Arif, F. Tahir, U. Fatima, R. Begum, Z. H. Farooqi, M. Shahid, T. Ahmad, M. Faizan, K. Naseem and Z. Ali, *Mater. Today Commun.*, 2022, **33**, 104700.
33 N. George, J. Joy, B. Mathew and E. P. Koshy, *J. Sol–Gel Sci. Technol.*, 2023, **107**, 685–696.
34 Z. H. Farooqi, G. T. Vladisavljević, N. Pamme, A. Fatima, R. Begum, A. Irfan and M. Chen, *Crit. Rev. Anal. Chem.*, 2023, 1–15, DOI: **10.1080/10408347.2023.2177097**.
35 E. Jha, P. Patel, P. Kumari, K. K. Verma, P. K. Panda, P. S. Mohanty, S. Patro, R. S. Varma, Y. K. Mishra, N. K. Kaushik, M. Suar and S. K. Verma, *J. Environ. Chem. Eng.*, 2023, **11**, 111183.
36 A. Raza, S. Rauf Khan, S. Ali, S. Jamil and S. Bibi, *Inorg. Chem. Commun.*, 2023, **153**, 110851.
37 A. Biffis, N. Orlandi and B. Corain, *Adv. Mater.*, 2003, **15**, 1551–1555.
38 B. Devadas, M. Prokop, S. Duraisamy and K. Bouzek, *Electrochim. Acta*, 2023, **441**, 141737.
39 X. Li, J. Iocozzia, Y. Chen, S. Zhao, X. Cui, W. Wang, H. Yu, S. Lin and Z. Lin, *Angew. Chem., Int. Ed.*, 2018, **57**, 2046–2070.
40 W. Zhan, Y. Shu, Y. Sheng, H. Zhu, Y. Guo, L. Wang, Y. Guo, J. Zhang, G. Lu and S. Dai, *Angew. Chem., Int. Ed.*, 2017, **56**, 4494–4498.
41 M. Arif, M. Shahid, A. Irfan, X. Wang, H. Noor, Z. H. Farooqi and R. Begum, *Inorg. Chem. Commun.*, 2022, **144**, 109870.
42 M. Arif, *Mater. Today Commun.*, 2023, **36**, 106580.
43 M. Arif, M. Shahid, A. Irfan, J. Nisar, W. Wu, Z. H. Farooqi and R. Begum, *RSC Adv.*, 2022, **12**, 5105–5117.
44 Z. Zhai, Q. Wu, J. Li, B. Zhou, J. Shen, Z. H. Farooqi and W. Wu, *J. Catal.*, 2019, **369**, 462–468.
45 M. Arif, Z. H. Farooqi, A. Irfan and R. Begum, *J. Mol. Liq.*, 2021, **336**, 116270.
46 S. Ashraf, R. Begum, R. Rehan, W. Wu and Z. H. Farooqi, *J. Inorg. Organomet. Polym. Mater.*, 2018, **28**, 1872–1884.
47 R. Chen, J. Shi, C. Liu, J. Li and S. Cao, *Adv. Compos. Hybrid Mater.*, 2022, **5**, 2223–2234.
48 S. Wang, A. Wang, Y. Ma, Q. Han, Y. Chen, X. Li, S. Wu, J. Li, S. Bai and J. Yin, *Biomater. Sci.*, 2021, **9**, 774–779.
49 F. Rastegar and M. Fallahi-Samberan, *Mater. Chem. Phys.*, 2024, **316**, 129042.
50 M. Arif, M. Shahid, A. Irfan, J. Nisar, X. Wang, N. Batool, M. Ali, Z. H. Farooqi and R. Begum, *Z. Phys. Chem.*, 2022, **236**, 1219–1241.
51 M. Shahid, Z. H. Farooqi, R. Begum, M. Arif, M. Azam, A. Irfan and U. Farooq, *Z. Phys. Chem.*, 2022, **236**, 87–105.
52 M. Arif, H. Raza and S. M. Haroon, *JOM*, 2023, **75**, 5217–5234.
53 M. Arif, *RSC Adv.*, 2022, **12**, 15447–15460.
54 K. Naseem, R. Begum and Z. H. Farooqi, *Polym. Compos.*, 2018, **39**, 2167–2180.
55 R. Begum, K. Naseem and Z. H. Farooqi, *J. Sol–Gel Sci. Technol.*, 2016, **77**, 497–515.
56 G. Mustafa, P. Ghosh Roy, S. Zhou, A. Irfan, A. R. Chaudhry, R. Begum and Z. H. Farooqi, *J. Mol. Liq.*, 2023, **385**, 122397.
57 K. Chang, Y. Yan, D. Zhang, Y. Xia, X. Chen, L. Lei and S. Shi, *Langmuir*, 2023, **39**, 2408–2421.
58 K. Naseem, R. Begum, Z. H. Farooqi, W. Wu and A. Irfan, *Appl. Organomet. Chem.*, 2020, **34**, e5742.
59 A. Ahmad, P. G. Roy, S. Zhou, A. Irfan, F. Kanwal, R. Begum and Z. H. Farooqi, *Int. J. Biol. Macromol.*, 2023, **240**, 124401.
60 X. Wang, X. Guo, M. A. Cohen Stuart, J. Wang and P. Ding, *Polymers*, 2023, **15**, 1935.
61 M. Arif, *RSC Adv.*, 2023, **13**, 3008–3019.
62 X. Xu, R. M. Sarhan, S. Mei, Z. Kochovski, W. Koopman, R. D. Priestley and Y. Lu, *ACS Appl. Mater. Interfaces*, 2023, **15**, 48623–48631.
63 A. Haleem, S. B. Syaal, M. Ajmal, J. Ambreen, S. Rauf, N. Ali, S. Muhammad, A. Shah, M. A. Zia and M. Siddiq, *Korean J. Chem. Eng.*, 2020, **37**, 614–622.
64 P. Agnihotri and A. Dan, *ACS Appl. Nano Mater.*, 2022, **5**, 10504–10515.
65 B. Wang, L. Dai, G. Yang, G. Bendrich, Y. Ni and G. Fang, *Carbohydr. Polym.*, 2019, **226**, 115289.
66 S. Mizuno, T.-A. Asoh, Y. Takashima, A. Harada and H. Uyama, *Chem. Commun.*, 2020, **56**, 14408–14411.
67 A. M. Atta, A. K. Gafer, H. A. Al-Lohedan, M. M. S. Abdullah, A. M. Tawfeek and A. O. Ezzat, *Molecules*, 2019, **24**, 3867.
68 X. Zhou, F. Chen, H. Lu, L. Kong, S. Zhang, W. Zhang, J. Nie, B. Du and X. Wang, *Ind. Eng. Chem. Res.*, 2019, **58**, 10922–10930.

69 T. Hou, S. S. Sana, D. V. Kumbhakar, H. Li, V. K. N. Boya, M. Aly Saad Aly, Z. Zhang and T. D. Pham, *J. Drug Delivery Sci. Technol.*, 2023, **87**, 104799.
70 K. Seku, G. Bhagavanth Reddy, S. S. Hussaini, B. Pejjai, M. Hussain, D. M. Reddy, M. A. K. Khazaleh and G. Mangatayaru, *Int. J. Biol. Macromol.*, 2022, **209**, 912–922.
71 B. Mutharani, P. Ranganathan, S.-M. Chen and C. Karuppiah, *Microchim. Acta*, 2019, **186**, 167.
72 Y. Tang, Y. Ding, T. Wu, L. Lv and Z. Yan, *Sens. Actuators, B*, 2016, **228**, 767–773.
73 G.-F. Gui, Y. Zhuo, Y.-Q. Chai, Y. Xiang and R. Yuan, *Biosens. Bioelectron.*, 2016, **77**, 7–12.
74 P. Bhol and P. S. Mohanty, *J. Phys.: Condens. Matter*, 2020, **33**, 084002.
75 L. Tzounis, M. Doña, J. M. Lopez-Romero, A. Fery and R. Contreras-Caceres, *ACS Appl. Mater. Interfaces*, 2019, **11**, 29360–29372.
76 M. Ajmal, M. Siddiq, N. Aktas and N. Sahiner, *RSC Adv.*, 2015, **5**, 43873–43884.
77 F. Bibi, M. Ajmal, F. Naseer, Z. H. Farooqi and M. Siddiq, *Int. J. Environ. Sci. Technol.*, 2017, **15**, 863–874.
78 H. Cai, X. Dai, X. Wang, P. Tan, L. Gu, Q. Luo, X. Zheng, Z. Li, H. Zhu, H. Zhang, Z. Gu, Q. Gong and K. Luo, *Adv. Sci.*, 2020, **7**, 1903243.
79 M. Arif, *J. Mol. Liq.*, 2023, **375**, 121346.
80 C. Alarcón-Fernández, M. Doña, A. Tapia-Fernández, G. Villaverde, M. R. Lopez-Ramirez, J. M. López-Romero and R. Contreras-Caceres, *ACS Appl. Nano Mater.*, 2020, **3**, 8247–8256.
81 M. Wei and M. J. Serpe, *Part. Part. Syst. Charact.*, 2019, **36**, 1800326.
82 L. Li, R. Niu and Y. Zhang, *RSC Adv.*, 2018, **8**, 12428–12438.
83 B. Tadgell, E. Ponomareva, M. Karg and P. Mulvaney, *J. Phys. Chem. C*, 2022, **126**, 15336–15347.
84 T. Ye, X. Jiang, W. Xu, M. Zhou, Y. Hu and W. Wu, *Polym. Chem.*, 2014, **5**, 2352–2362.
85 K. Rajar and E. Alveroglu, *J. Mol. Struct.*, 2017, **1146**, 592–599.
86 M. Zhang and W. Zhang, *J. Phys. Chem. C*, 2008, **112**, 6245–6252.
87 K. Naseem, Z. H. Farooqi, R. Begum, W. Wu, A. Irfan and A. G. Al-Sehemi, *Macromol. Chem. Phys.*, 2018, **219**, 1800211.
88 I. Hussain, M. Shahid, F. Ali, A. Irfan, R. Begum and Z. H. Farooqi, *Environ. Technol.*, 2023, **44**, 1679–1689.
89 Y. Lu, J. Yuan, F. Polzer, M. Drechsler and J. Preussner, *ACS Nano*, 2010, **4**, 7078–7086.
90 P. Boonying, S. Martwiset and S. Amnuaypanich, *Appl. Nanosci.*, 2018, **8**, 475–488.
91 K. Naseem, R. Begum, W. Wu, A. Irfan, A. G. Al-Sehemi and Z. H. Farooqi, *J. Cleaner Prod.*, 2019, **211**, 855–864.
92 Y. Lu, S. Proch, M. Schrinner, M. Drechsler, R. Kempe and M. Ballauff, *J. Mater. Chem.*, 2009, **19**, 3955–3961.
93 N. Tan, C. Lee and P. Li, *Polymers*, 2016, **8**, 105.
94 T. Zhang, L. Li, Z. Ye, Q. Yang, Y. Tian and X. Guo, *RSC Adv.*, 2018, **8**, 18252–18259.
95 B. Hu, T. Wu, K. Ding, X. Zhou, T. Jiang and B. Han, *J. Phys. Chem. C*, 2010, **114**, 3396–3400.
96 G. Liu, D. Wang, F. Zhou and W. Liu, *Small*, 2015, **11**, 2807–2816.
97 A. Mohan, J. Peter, L. Rout, A. M. Thomas, S. Nagappan, S. Parambadath, W. Zhang, M. Selvaraj and C.-S. Ha, *Colloids Surf., A*, 2021, **611**, 125846.
98 M. R. Nabid, Y. Bide and M. Niknezhad, *ChemCatChem*, 2014, **6**, 538–546.
99 J. Yang, D. Wang, W. Liu, X. Zhang, F. Bian and W. Yu, *Green Chem.*, 2013, **15**, 3429–3437.
100 N. Sahiner and A. O. Yasar, *Fuel Process. Technol.*, 2016, **144**, 124–131.
101 Y. Mei, Y. Lu, F. Polzer, M. Ballauff and M. Drechsler, *Chem. Mater.*, 2007, **19**, 1062–1069.
102 R. J. Rauschendorfer, K. M. Whitham, S. Summer, S. A. Patrick, A. E. Pierce, H. Sefi-Cyr, S. Tadjiki, M. D. Kraft, S. R. Emory, D. A. Rider and M. D. Montaño, *Front. Toxicol.*, 2021, **3**, 1–14.
103 T. Kureha, Y. Nagase and D. Suzuki, *ACS Omega*, 2018, **3**, 6158–6165.
104 D. Suzuki and H. Kawaguchi, *Langmuir*, 2005, **21**, 12016–12024.
105 T. Curtis, A. K. Taylor, S. E. Alden, C. Swanson, J. Lo, L. Knight, A. Silva, B. D. Gates, S. R. Emory and D. A. Rider, *ACS Omega*, 2018, **3**, 10572–10588.
106 M. Bradley and B. S. Garcia-Risueño, *J. Colloid Interface Sci.*, 2011, **355**, 321–327.
107 M. Karg, I. Pastoriza-Santos, J. Pérez-Juste, T. Hellweg and L. M. Liz-Marzán, *Small*, 2007, **3**, 1222–1229.
108 J. E. Wong, A. K. Gaharwar, D. Müller-Schulte, D. Bahadur and W. Richtering, *J. Colloid Interface Sci.*, 2008, **324**, 47–54.
109 M. Karg, Y. Lu, E. Carbó-Argibay, I. Pastoriza-Santos, J. Pérez-Juste, L. M. Liz-Marzán and T. Hellweg, *Langmuir*, 2009, **25**, 3163–3167.
110 S. Mohammed Safiullah, K. Abdul Wasi and K. Anver Basha, *Appl. Surf. Sci.*, 2015, **357**, 112–121.
111 J. Su, S. Wang, Z. Xu, G. Wu, L. Wang and X. Huang, *Chem. Commun.*, 2019, **55**, 10760–10763.
112 A. C. Manikas, A. Papa, F. Causa, G. Romeo and P. A. Netti, *RSC Adv.*, 2015, **5**, 13507–13512.
113 X. He, Z. Liu, F. Fan, S. Qiang, L. Cheng and W. Yang, *J. Nanopart. Res.*, 2015, **17**, 74.
114 G. Li, X. Yang, B. Wang, J. Wang and X. Yang, *Polymer*, 2008, **49**, 3436–3443.
115 R. Begum, K. Naseem, E. Ahmed, A. Sharif and Z. H. Farooqi, *Colloids Surf., A*, 2016, **511**, 17–26.
116 S. Iqbal, N. Iqbal, S. Musaddiq, Z. H. Farooqi, M. A. Habila, S. M. Wabaidur and A. Iqbal, *Heliyon*, 2024, **10**, E25385.
117 M. Riaz, M. Ajmal, A. Naseem, N. Jabeen, Z. H. Farooqi, K. Mahmood, A. Ali, L. Rasheed and A. N. S. Saqib, *Z. Phys. Chem.*, 2022, **236**, 1441–1460.
118 Z. H. Farooqi, H. Sultana, R. Begum, M. Usman, M. Ajmal, J. Nisar, A. Irfan and M. Azam, *Int. J. Environ. Anal. Chem.*, 2022, **102**, 4104–4120.
119 J. Ambreen, F. F. Al-Harbi, H. Sakhawat, M. Ajmal, H. Naeem, Z. H. Farooqi, N. Batool and M. Siddiq, *J. Mol. Liq.*, 2022, **355**, 118931.

120 A. Yoshida, Y. Kitayama, K. Kiguchi, T. Yamada, H. Akasaka, R. Sasaki and T. Takeuchi, *ACS Appl. Bio Mater.*, 2019, **2**, 1177–1183.
121 A. Contin, A. Biffis, S. Sterchele, K. Dörmbach, S. Schipmann and A. Pich, *J. Colloid Interface Sci.*, 2014, **414**, 41–45.
122 S. Li, X. Wang, J. Chen, J. Guo, M. Yuan, G. Wan, C. Yan, W. Li, H.-G. Machens, Y. Rinkevich, X. Yang, H. Song and Z. Chen, *Int. J. Biol. Macromol.*, 2022, **202**, 657–670.
123 T. M. Ansari, M. Ajmal, S. Saeed, H. Naeem, H. B. Ahmad, K. Mahmood and Z. H. Farooqi, *J. Iran. Chem. Soc.*, 2019, **16**, 2765–2776.
124 S. Rahman, F. F. Al-Harbi, M. Ajmal, A. Naseem, Z. H. Farooqi and M. Siddiq, *J. Mater. Sci.*, 2022, **57**, 6763–6779.
125 A. M. Al-Enizi, T. Ahamad, A. B. Al-hajji, J. Ahmed, A. A. Chaudhary and S. M. Alshehri, *Int. J. Biol. Macromol.*, 2018, **109**, 803–809.
126 J. T. Zhang, G. Wei, T. F. Keller, H. Gallagher, C. Stötzel, F. A. Müller, M. Gottschaldt, U. S. Schubert and K. D. Jandt, *Macromol. Mater. Eng.*, 2010, **295**, 1049–1057.
127 X. Liu, C. Zhang, J. Yang, D. Lin, L. Zhang, X. Chen and L. Zha, *RSC Adv.*, 2013, **3**, 3384–3390.
128 X.-J. Zhou, H.-P. Lu, L.-L. Kong, D. Zhang, W. Zhang, J.-J. Nie, J.-Y. Yuan, B.-Y. Du and X.-P. Wang, *Chin. J. Polym. Sci.*, 2019, **37**, 235–242.
129 F. Naseer, M. Ajmal, F. Bibi, Z. H. Farooqi and M. Siddiq, *Polym. Compos.*, 2018, **39**, 3187–3198.
130 T. Nakao, D. Nagao, H. Ishii and M. Konno, *Colloids Surf., A*, 2014, **446**, 134–138.
131 Z. Shafiq, M. Ajmal, S. Kiran, S. Zulfiqar, G. Yasmeen, M. Iqbal, Z. H. Farooqi, Z. Ahmad, N. Sahiner, K. Mahmood, H. B. Ahmad and A. Al-Harrasi, *Pure Appl. Chem.*, 2019, **91**, 1567–1582.
132 S. Sharma, Deepak, A. Kumar, S. Afgan and R. Kumar, *ChemistrySelect*, 2017, **2**, 11281–11287.
133 S. Iqbal, S. Musaddiq, R. Begum, A. Irfan, Z. Ahmad, M. Azam, J. Nisar and Z. H. Farooqi, *Z. Phys. Chem.*, 2021, **235**, 1701–1719.
134 S. ur Rehman, M. Siddiq, H. Al-Lohedan and N. Sahiner, *Chem. Eng. J.*, 2015, **265**, 201–209.
135 B. Mutharani, T.-W. Chen, S.-M. Chen and X. Liu, *Sens. Actuators, B*, 2020, **316**, 128103.
136 K. Wiemer, K. Dörmbach, I. Slabu, G. Agrawal, F. Schrader, T. Caumanns, S. D. M. Bourone, J. Mayer, J. Steitz, U. Simon and A. Pich, *J. Mater. Chem. B*, 2017, **5**, 1284–1292.
137 N. A. Nemygina, L. Z. Nikoshvili, I. Y. Tiamina, A. V. Bykov, I. S. Smirnov, T. Lagrange, Z. Kaszkur, V. G. Matveeva, E. M. Sulman and L. Kiwi-Minsker, *Org. Process Res. Dev.*, 2018, **22**, 1606–1613.
138 S. Afridi, L. A. Shah, M. Khan, S. A. Khan and D. Ye, *Polym. Bull.*, 2023, **80**, 8259–8281.
139 M. U. Kakar, K. Khan, M. Akram, R. Sami, E. Khojah, I. Iqbal, M. Helal, A. Hakeem, Y. Deng and R. Dai, *Sci. Rep.*, 2021, **11**, 14759.
140 M. N. Nadagouda and R. S. Varma, *Macromol. Rapid Commun.*, 2007, **28**, 465–472.
141 N. Sahiner, *Colloid Polym. Sci.*, 2006, **285**, 283–292.
142 A. Basu, I. Tolbatov, A. Marrone, A. Vaskevich and L. Chuntonov, *J. Phys. Chem. C*, 2024, **128**, 3438–3448.
143 M. Chen, G. Bolognesi, R. Begum, Z. H. Farooqi and G. T. Vladisavljević, *Emergent Mater.*, 2024, 1–13.
144 S. Bandyopadhyay, A. Sharma and W. Glomm, *Gels*, 2017, **3**, 42.
145 S. Zahid, A. K. Alzahrani, N. Kizilbash, J. Ambreen, M. Ajmal, Z. H. Farooqi and M. Siddiq, *RSC Adv.*, 2022, **12**, 33215–33228.
146 H. Naeem, M. Ajmal, S. Z. Khan, M. N. Ashiq and M. Siddiq, *Soft Mater.*, 2021, **19**, 480–494.
147 N. Jabeen, Z. H. Farooqi, A. Shah, A. Ali, M. Khurram, K. Mahmood, N. Sahiner and M. Ajmal, *J. Porous Mater.*, 2021, **1**, 1–14.
148 Z. H. Farooqi, S. Iqbal, S. R. Khan, F. Kanwal and R. Begum, *e-Polymers*, 2014, **14**, 313–321.
149 R. Begum, Z. H. Farooqi, J. Xiao, E. Ahmed, A. Sharif and A. Irfan, *J. Mol. Liq.*, 2021, **338**, 116780.
150 M. Tercan, S. De Mirci, O. Dayan and N. Sahiner, *New J. Chem.*, 2020, **44**, 4417–4425.
151 R. Begum, Z. H. Farooqi, A. H. Aboo, E. Ahmed, A. Sharif and J. Xiao, *J. Hazard. Mater.*, 2019, **377**, 399–408.
152 L. A. Shah, M. Sayed and M. Siddiq, *Mater. Sci.–Pol.*, 2017, **35**, 651–659.
153 G. Youzhi, H. Yang, Z. Yiping, C. Li and Y. Fanyong, *J. Mater. Sci.*, 2016, **51**, 3200–3210.
154 M. Ajmal, S. Demirci, M. Siddiq, N. Aktas and N. Sahiner, *New J. Chem.*, 2016, **40**, 1485–1496.
155 T. Chen, Q. Fang, L. Zhou, Z. Xu, J. Qiu, M. Wang and J. Wang, *React. Funct. Polym.*, 2019, **142**, 104–111.
156 M. Ajmal, M. Siddiq, H. Al-Lohedan and N. Sahiner, *RSC Adv.*, 2014, **4**, 59562–59570.
157 Y. Meng, J. Yin, T. Jiao, J. Bai, L. Zhang, J. Su, S. Liu, Z. Bai, M. Cao and Q. Peng, *J. Mol. Liq.*, 2020, **298**, 112010.
158 O. Ramírez, S. Bonardd, C. Saldías, Y. Zambrano, D. D. Díaz and A. Leiva, *Carbohydr. Polym.*, 2022, **297**, 120021.
159 R. Contreras-Caceres, P. Alonso-Cristobal, D. Mendez-Gonzalez, M. Laurenti, A. Maldonado-Valdivia, F. Garcia-Blanco, E. López Cabarcos, A. Fernandez-Barbero, J. M. Lopez-Romero and J. Rubio-Retama, *Langmuir*, 2014, **30**, 15560–15567.
160 M. E. Villanueva, A. M. D. R. Diez, J. A. González, C. J. Pérez, M. Orrego, L. Piehl, S. Teves and G. J. Copello, *ACS Appl. Mater. Interfaces*, 2016, **8**, 16280–16288.
161 M. Wei and M. J. Serpe, *Part. Part. Syst. Charact.*, 2019, **36**, 1800326.
162 K. Virk, K. Sharma, S. Kapil, V. Kumar, V. Sharma, S. Pandey and V. Kumar, *J. Polym. Res.*, 2022, **29**, 1–15.
163 E. M. Bakhsh, M. S. J. Khan, K. Akhtar, S. B. Khan and A. M. Asiri, *Appl. Organomet. Chem.*, 2022, **36**, e6741.
164 J. Ding, Q. Li, X. Xu, X. Zhang, Y. Su, Q. Yue and B. Gao, *Carbohydr. Polym.*, 2018, **190**, 12–22.
165 P. Gu, J. Wang, P. Müller-Buschbaum, D. Qi and Q. Zhong, *ACS Appl. Mater. Interfaces*, 2020, **12**, 34180–34189.
166 Z. Chen, L. Hu and M. J. Serpe, *J. Mater. Chem.*, 2012, **22**, 20998–21002.

167 W. Liu, H. Cai, P. Lu, Q. Xu, Y. Zhongfu and J. Dong, *Int. J. Hydrogen Energy*, 2013, **38**, 9206–9216.
168 A. Gibb, A. Vorobjovs, Z. Jagoda, J. Winiarski and A. Stankiewicz, *Trans. IMF*, 2020, **98**, 15–20.
169 Z. H. Farooqi and M. Siddiq, *J. Dispersion Sci. Technol.*, 2015, **36**, 423–429.
170 X. Dong, S. Chen, J. Zhou, L. Wang and L. Zha, *Mater. Des.*, 2016, **104**, 303–311.
171 B. Li, X. Chen, K. Li, C. Zhang, Y. He, R. Du, J. Wang and L. Chen, *J. Ind. Eng. Chem.*, 2019, **78**, 198–209.
172 N. Sahiner and S. Yildiz, *Fuel Process. Technol.*, 2014, **126**, 324–331.
173 Y. Gotoh, R. Igarashi, Y. Ohkoshi, M. Nagura, K. Akamatsu and S. Deki, *J. Mater. Chem.*, 2000, **10**, 2548–2552.
174 H. Park, L. Srisombat, A. Jamison, T. Liu, M. Marquez, H. Park, S. Lee, T.-C. Lee and T. Lee, *Gels*, 2018, **4**, 28.
175 F. Mou, C. Chen, Q. Zhong, Y. Yin, H. Ma and J. Guan, *ACS Appl. Mater. Interfaces*, 2014, **6**, 9897–9903.
176 A. Saad, R. Mills, H. Wan, L. Ormsbee and D. Bhattacharyya, *Ind. Eng. Chem. Res.*, 2020, **59**, 16614–16625.
177 E. Menard, K. J. Lee, D. Khang, R. G. Nuzzo, J. A. Rogers, A. Rogers, Z. Bao, K. Baldwin, A. Dodabalapur, B. Crone, V. R. Raju, V. Kuck, H. Katz, K. Amundson, J. Ewing, P. Drzaic, G. Kane, J. Campi, M. S. Hammond, F. P. Cuomo, B. Greening, C. D. Sheraw, J. A. Nichols, D. J. Gundlach, J. R. Huang, C. C. Kuo, L. Jia, H. Klauk, T. N. Jackson, E. Burns, C. Kuhn, K. Jacobs, J. D. Mackenzie, C. Ramsdale, A. C. Arias, J. Watts, M. Etchells, K. Chalmers, P. Devine, N. Murton, S. Norval, J. King, J. Mills, H. Sirringhaus, R. H. Friend, J. Soc Inf, B. Jiguang Zhang, S. Xu, E. Kumacheva, E. Kumacheva, J. Zhang and S. Xu, *Adv. Mater.*, 2005, **17**, 2336–2340.
178 S. Pourbeyram and S. Mohammadi, *J. Non-Cryst. Solids*, 2014, **402**, 58–63.
179 M. Ajmal, F. Aftab, I. Bibi, M. Iqbal, J. Ambreen, H. B. Ahmad, N. Akhtar, A. Haleem and M. Siddiq, *J. Porous Mater.*, 2019, **26**, 281–290.
180 O. Ozay, N. Aktas, E. Inger and N. Sahiner, *Int. J. Hydrogen Energy*, 2011, **36**, 1998–2006.
181 N. Sahiner, *Colloids Surf., A*, 2013, **433**, 212–218.
182 B. Li, X. Chen, Y. Ma, J. Wang, X. Zhai, Y. He, Y. Li, R. Ma and W. Zhang, *J. Environ. Chem. Eng.*, 2021, **9**, 104757.
183 Y. Tang, T. Wu, B. Hu, Q. Yang, L. Liu, B. Yu, Y. Ding and S. Ye, *Mater. Chem. Phys.*, 2015, **149–150**, 460–466.
184 L. Y. Chen, C. M. Ou, W. Y. Chen, C. C. Huang and H. T. Chang, *ACS Appl. Mater. Interfaces*, 2013, **5**, 4383–4388.
185 Y.-Y. Liu, X.-Y. Liu, J.-M. Yang, D.-L. Lin, X. Chen and L.-S. Zha, *Colloids Surf., A*, 2012, **393**, 105–110.
186 A. Sánchez-Iglesias, M. Grzelczak, B. Rodríguez-González, P. Guardia-Girós, I. Pastoriza-Santos, J. Pérez-Juste, M. Prato and L. M. Liz-Marzán, *ACS Nano*, 2009, **3**, 3184–3190.
187 K. Khan, A. J. Shaikh, M. Siddiq, T. A. Sherazi and M. Nawaz, *J. Polym. Eng.*, 2016, **36**, 287–292.
188 C. Fernández-López, L. Polavarapu, D. M. Solís, J. M. Taboada, F. Obelleiro, R. Contreras-Cáceres, I. Pastoriza-Santos and J. Pérez-Juste, *ACS Appl. Mater. Interfaces*, 2015, **7**, 12530–12538.
189 V. Sabadasch, L. Wiehemeier, T. Kottke and T. Hellweg, *Soft Matter*, 2020, **16**, 5422–5430.
190 A. C. Manikas, A. Aliberti, F. Causa, E. Battista and P. A. Netti, *J. Mater. Chem. B*, 2015, **3**, 53–58.
191 V. K. Saruchi, J. K. Dhami, V. Rehani and M. Singh, *J. Polym. Res.*, 2022, **29**, 1–14.
192 H. Zhang, S. Guo, S. Fu and Y. Zhao, *Polymers*, 2017, **9**, 238.
193 J. Liu, J. Wang, Y. Wang, C. Liu, M. Jin, Y. Xu, L. Li, X. Guo, A. Hu, T. Liu, S. F. Lincoln and R. K. Prud'homme, *Colloids Interface Sci. Commun.*, 2015, **4**, 1–4.
194 J. Machotová, J. Šňupárek, L. Prokůpek, T. Rychlý and P. Vlasák, *Prog. Org. Coat.*, 2008, **63**, 175–181.
195 Q. Chen, K. Xu, W. Zhang, C. Song and P. Wang, *Colloid Polym. Sci.*, 2009, **287**, 1339–1346.
196 O. Güven, S. Demirci, S. D. Sütekin, B. Ari and N. Sahiner, *Radiat. Phys. Chem.*, 2022, **198**, 110217.
197 Z. H. Farooqi, Z. Butt, R. Begum, S. R. Khan, A. Sharif and E. Ahmed, *Mater. Sci.–Pol.*, 2015, **33**, 627–634.
198 Y. Dong, Y. Jin, J. Wang, J. Shu and M. Zhang, *Chem. Eng. J.*, 2017, **324**, 303–312.
199 N. Sahiner and A. O. Yasar, *Int. J. Hydrogen Energy*, 2013, **38**, 6736–6743.
200 R. Vescovo, M. Becker, M. M. Natile, P. Canton, C. Evangelisti and A. Biffis, *ACS Appl. Nano Mater.*, 2021, **4**, 8343–8351.
201 S. Wang, Y. Mo, T. Vincent, J. C. Roux, E. Rodríguez-Castellón, C. Faur and E. Guibal, *J. Mater. Sci.*, 2020, **55**, 2032–2051.
202 M. R. Nabid, Y. Bide, E. Aghaghafari and S. J. T. Rezaei, *Catal. Lett.*, 2014, **144**, 355–363.
203 N. S. Reddy, S. Eswaramma, I. Chung, K. S. V. K. Rao, P. Ramesh and A. Chandra Sekhar, *Int. J. Polym. Mater. Polym. Biomater.*, 2019, **68**, 870–880.
204 J. Cao, J. Li, Y. Chen, L. Zhang and J. Zhou, *Adv. Funct. Mater.*, 2018, **28**, 1800739.
205 Y. Zheng, F. Cheng and W. He, *Colloids Surf., A*, 2019, **575**, 94–101.
206 J. Zhang, N. Ma, F. Tang, Q. Cui, F. He and L. Li, *ACS Appl. Mater. Interfaces*, 2012, **4**, 1747–1751.
207 W. Wu, J. Shen, Y. Li, H. Zhu, P. Banerjee and S. Zhou, *Biomaterials*, 2012, **33**, 7115–7125.
208 W. Wu, N. Mitra, E. C. Y. Yan and S. Zhou, *ACS Nano*, 2010, **4**, 4831–4839.
209 Y. Zhang, Y. Zhang, K. Liu and Y. Guan, *RSC Adv.*, 2012, **2**, 4768–4776.
210 Y. Zuo, J. Zhao, Y. Gao and Y. Zhang, *J. Mater. Sci.*, 2017, **52**, 9584–9601.
211 M. S. Strozyk, M. Chanana, I. Pastoriza-Santos, J. Pérez-Juste and L. M. Liz-Marzán, *Adv. Funct. Mater.*, 2012, **22**, 1436–1444.
212 R. Javed, L. A. Shah, M. Sayed and M. S. Khan, *RSC Adv.*, 2018, **8**, 14787–14797.

213 M. Ajmal, S. Demirci, M. Siddiq, N. Aktas and N. Sahiner, *Colloids Surf., A*, 2015, **486**, 29–37.
214 M. Das, N. Sanson and E. Kumacheva, *Chem. Mater.*, 2008, **20**, 7157–7163.
215 S. R. Khan, S. Ali, B. Ullah, S. Jamil and T. Zanib, *J. Nanopart. Res.*, 2020, **22**, 1–12.
216 S. Iqbal, C. Zahoor, S. Musaddiq, M. Hussain, R. Begum, A. Irfan, M. Azam and Z. H. Farooqi, *Ecotoxicol. Environ. Saf.*, 2020, **202**, 110924.
217 P. Bhol, M. Mohanty and P. S. Mohanty, *J. Mol. Liq.*, 2021, **325**, 115135.
218 X. Chen, Y. An, D. Zhao, Z. He, Y. Zhang, J. Cheng and L. Shi, *Langmuir*, 2008, **24**, 8198–8204.
219 M. Bradley and B. Vincent, *Langmuir*, 2008, **24**, 2421–2425.
220 Y. M. Liu, X. J. Ju, Y. Xin, W. C. Zheng, W. Wang, J. Wei, R. Xie, Z. Liu and L. Y. Chu, *ACS Appl. Mater. Interfaces*, 2014, **6**, 9530–9542.
221 Y. Wang, N. Lin, Y. Gong, R. Wang and X. Zhang, *Chemosphere*, 2021, **280**, 130663.
222 A. Wang, Z. Liu, S. Li, Y. Liu, H. Zhao, Y. Liu, T. Ye, Y. Niu and W. Li, *J. Mol. Liq.*, 2021, **342**, 117572.
223 J. Paul Guin, Y. K. Bhardwaj and L. Varshney, *J. Appl. Polym. Sci.*, 2018, **135**, 46200.
224 Q. Zhou, M. Lei, Y. Wu, S. Li, Y. Tong, Z. Li, M. Liu, L. Guo and C. Chen, *Chemosphere*, 2021, **279**, 130584.
225 S. Demirci, K. Sel and N. Sahiner, *Sep. Purif. Technol.*, 2015, **155**, 66–74.
226 S. Dhanavel, N. Manivannan, N. Mathivanan, V. K. Gupta, V. Narayanan and A. Stephen, *J. Mol. Liq.*, 2018, **257**, 32–41.
227 Z. Wang, X. Chen, K. Li, S. Bi, C. Wu and L. Chen, *J. Membr. Sci.*, 2015, **496**, 95–107.
228 N. Sahiner, S. Yildiz, M. Sahiner, Z. A. Issa and H. Al-Lohedan, *Appl. Surf. Sci.*, 2015, **354**, 388–396.
229 L. Zhao, Q. Li, Y. Su, Q. Yue and B. Gao, *Int. J. Hydrogen Energy*, 2017, **42**, 6746–6756.
230 K. Naseem, A. Aziz, M. H. Tahir, A. Ameen, A. Ahmad, K. Ahmad, M. Arif, W. Hassan, J. Najeeb and E. Rao, *Int. J. Environ. Sci. Technol.*, 2024, **21**, 2163–2194.
231 T. Brändel, V. Sabadasch, Y. Hannappel and T. Hellweg, *ACS Omega*, 2019, **4**, 4636–4649.
232 Y. Dong, Y. Ma, T. Zhai, F. Shen, Y. Zeng, H. Fu and J. Yao, *Macromol. Rapid Commun.*, 2007, **28**, 2339–2345.
233 E. Wi, S. Go, S. Y. Shin, H. J. Cheon, G. Jeong, H. Cheon, J. Kim, H. R. Jung, H. Kim and M. Chang, *Chem. Eng. J.*, 2023, **454**, 140309.
234 C. Xiao, Q. Wu, A. Chang, Y. Peng, W. Xu and W. Wu, *J. Mater. Chem. A*, 2014, **2**, 9514–9523.
235 G. Kocak, *J. Appl. Polym. Sci.*, 2020, **137**, 48360.
236 N. Sahiner, O. Ozay, N. Aktas, E. Inger and J. He, *Int. J. Hydrogen Energy*, 2011, **36**, 15250–15258.
237 H. Ozay, P. Ilgin and O. Ozay, *Int. J. Hydrogen Energy*, 2020, **45**, 17613–17624.
238 H. Gholami Derami, P. Gupta, R. Gupta, P. Rathi, J. J. Morrissey and S. Singamaneni, *ACS Appl. Nano Mater.*, 2020, **3**, 5437–5448.
239 G. S. Tatykhanova, A. N. Klivenko, G. M. Kudaibergenova and S. E. Kudaibergenov, *Macromol. Symp.*, 2016, **363**, 49–56.
240 D. Ulker, C. Tuncer, S. B. Sezgin, Y. Toptas, A. Cabuk and V. Bütün, *J. Polym. Res.*, 2017, **24**, 169.
241 T. Gancheva and N. Virgilio, *ACS Appl. Mater. Interfaces*, 2018, **10**, 21073–21078.
242 P. Pongsanon, Y. Oota, A. Kawamura, H. Kawasaki and T. Miyata, *Macromolecules*, 2023, **56**, 9853–9865.
243 I. Hussain, Z. H. Farooqi, F. Ali, R. Begum, A. Irfan, W. Wu, X. Wang, M. Shahid and J. Nisar, *J. Mol. Liq.*, 2021, **335**, 116106.
244 X. Zhang, X. Lv, T. Xie, Y. Cheng, J. Zhang and X. Xu, *Eur. Polym. J.*, 2023, **200**, 112533.
245 Z. H. Farooqi, R. Begum, K. Naseem, U. Rubab, M. Usman, A. Khan and A. Ijaz, *Russ. J. Phys. Chem. A*, 2016, **90**, 2600–2608.
246 N. P. B. Tan and C. H. Lee, in *Green Chemical Processing and Synthesis*, InTech, 2017.
247 V. Melinte, L. Stroea, T. Buruiana and A. L. Chibac, *Eur. Polym. J.*, 2019, **121**, 109289.
248 M. Hashaam, S. Ali, T. Khan, M. Salman, S. R. Khan, A. I. Aqib, T. Zaheer, S. Bibi, S. Jamil, M. S. Al-Sharif, S. F. Mahmoud and W. Yao, *Catalysts*, 2022, **12**, 1172.
249 A. Raza, S. Rauf Khan, S. Ali, S. Jamil and S. Bibi, *Inorg. Chem. Commun.*, 2023, **153**, 110851.
250 L. A. Shah, A. Haleem, M. Sayed and M. Siddiq, *J. Environ. Chem. Eng.*, 2016, **4**, 3492–3497.
251 X. Han, X. Chen, M. Yan and H. Liu, *Particuology*, 2019, **44**, 63–70.
252 J. Cao, S. Mei, H. Jia, A. Ott, M. Ballauff and Y. Lu, *Langmuir*, 2015, **31**, 9483–9491.
253 P. N. Eyimegwu, J. A. Lartey and J.-H. Kim, *ACS Appl. Nano Mater.*, 2019, **2**, 6057–6066.
254 M. Albino, T. J. Burden, C. C. Piras, A. C. Whitwood, I. J. S. Fairlamb and D. K. Smith, *ACS Sustain. Chem. Eng.*, 2023, **11**, 1678–1689.
255 M. C. Hong, H. Ahn, M. C. Choi, Y. Lee, J. Kim and H. Rhee, *Appl. Organomet. Chem.*, 2014, **28**, 156–161.
256 P. A. Pourjavadi, N. Keshavarzi, F. M. Moghaddam and S. H. Hosseini, *ChemistrySelect*, 2018, **3**, 2716–2722.
257 D. Zhang, H. Li, J. Li, Z. Xu, H. Liu, Y. Zhao, X. Feng and L. Chen, *Appl. Surf. Sci.*, 2020, **512**, 145668.
258 F. Tang, N. Ma, L. Tong, F. He and L. Li, *Langmuir*, 2012, **28**, 883–888.
259 D. M. Han, Q. M. Zhang and M. J. Serpe, *Nanoscale*, 2015, **7**, 2784–2789.
260 Y. Tang, Y. Cao, S. Wang, G. Shen and R. Yu, *Sens. Actuators, B*, 2009, **137**, 736–740.
261 I. Gholamali, M. Asnaashariisfahani and E. Alipour, *Regener. Eng. Transl. Med.*, 2020, **6**, 138–153.
262 S. Batool, Z. Hussain, M. B. K. Niazi, U. Liaqat and M. Afzal, *J. Drug Delivery Sci. Technol.*, 2019, **52**, 403–414.
263 W. Wu, J. Shen, P. Banerjee and S. Zhou, *Biomaterials*, 2010, **31**, 7555–7566.
264 W. Wu, J. Shen, P. Banerjee and S. Zhou, *Biomaterials*, 2011, **32**, 598–609.

265 S. Mane, S. Ponrathnam and N. Chavan, *Int. J. Polym. Mater.*, 2016, **65**, 285–293.
266 I. O. de Solorzano, M. Prieto, G. Mendoza, V. Sebastian and M. Arruebo, *Nanomedicine*, 2020, **15**, 219–234.
267 N. S. V. Capanema, I. C. Carvalho, A. A. P. Mansur, S. M. Carvalho, A. P. Lage and H. S. Mansur, *ACS Appl. Nano Mater.*, 2019, **2**, 7393–7408.
268 A. Seyfoori, S. A. Seyyed Ebrahimi, E. Samiei and M. Akbari, *ACS Appl. Mater. Interfaces*, 2019, **11**, 24945–24958.
269 M. C. Galdioli Pellá, A. R. Simão, M. K. Lima-Tenório, E. Tenório-Neto, D. B. Scariot, C. V. Nakamura and A. F. Rubira, *Carbohydr. Polym.*, 2020, **239**, 116236.
270 A. Wang, J. Li, Q. Dong, S. Wang, H. Jian, M. Wang, P. Ren and S. Bai, *ACS Appl. Mater. Interfaces*, 2019, **11**, 4408–4415.
271 A. Haleem, S. Q. Chen, M. Ullah, M. Siddiq and W. D. He, *J. Environ. Chem. Eng.*, 2021, **9**, 106510.
272 G. M. Raghavendra, T. Jayaramudu, K. Varaprasad, G. S. Mohan Reddy and K. M. Raju, *RSC Adv.*, 2015, **5**, 14351–14358.
273 C. Marambio-Jones and E. M. V. Hoek, *J. Nanopart. Res.*, 2010, **12**, 1531–1551.
274 J. R. Morones, J. L. Elechiguerra, A. Camacho, K. Holt, J. B. Kouri, J. T. Ramírez and M. J. Yacaman, *Nanotechnology*, 2005, **16**, 2346–2353.
275 D. M. Suflet, I. Popescu, I. M. Pelin, D. L. Ichim, O. M. Daraba, M. Constantin and G. Fundueanu, *Pharmaceutics*, 2021, **13**, 1461.
276 N. Häntzschel, R. D. Hund, H. Hund, M. Schrinner, C. Lück and A. Pich, *Macromol. Biosci.*, 2009, **9**, 444–449.
277 M. Sabzi, M. J. Afshari, M. Babaahmadi and N. Shafagh, *Colloids Surf., B*, 2020, **188**, 110757.
278 M. T. S. Alcântara, N. Lincopan, P. M. Santos, P. A. Ramirez, A. J. C. Brant, H. G. Riella and A. B. Lugão, *Radiat. Phys. Chem.*, 2020, **169**, 108777.
279 M. R. El-Aassar, O. M. Ibrahim, M. M. G. Fouda, H. Fakhry, J. Ajarem, S. N. Maodaa, A. A. Allam and E. E. Hafez, *Carbohydr. Polym.*, 2021, **255**, 117484.
280 H. E. Salama, G. R. Saad and M. W. Sabaa, *J. Biomater. Sci., Polym. Ed.*, 2016, **27**, 1880–1898.
281 C. Ryan, E. Alcock, F. Buttimer, M. Schmidt, D. Clarke, M. Pemble and M. Bardosova, *Sci. Technol. Adv. Mater.*, 2017, **18**, 528–540.
282 V. Thomas, M. M. Yallapu, B. Sreedhar and S. K. Bajpai, *J. Colloid Interface Sci.*, 2007, **315**, 389–395.